DNA Adsorption, Desorption, and Fluorescence Quenching by Graphene Oxide and Related Analytical Application

by

Po-Jung Huang

A thesis
presented to the University of Waterloo
in fulfillment of the
thesis requirement for the degree of
Master of Science
in
Chemistry

Waterloo, Ontario, Canada, 2011

Author's Declaration

I hereby declare that I am the sole author of this thesis. This is a true copy of the thesis, including any required final revisions, as accepted by my examiners.

I understand that my thesis may be made electronically available to the public.

Abstract

Graphene is a single layer of graphite with many unique mechanical, electrical, and optical properties. In addition, graphene is also known to adsorb wide range of biomolecules including single-stranded DNA. On the other hand, the adsorption of double-stranded DNA was much weaker. To properly disperse in water, graphene oxide (GO) is often used due to its oxygen-containing groups on the surface. Recently, it was discovered that it could efficiently quench the fluorescence of fluorophores that were adsorbed. With these properties, it is possible to prepare DNA-based optical sensors using GO. Majority of the DNA/GO-based fluorescent sensors reported so far were relied on the complete desorption of DNA probes. Even though all these reports demonstrated the sensitivity and selectivity of the system, the fundamentals of binding between DNA and GO were hardly addressed.

Understanding and controlling binding between biomolecules and inorganic materials is very important in biosensor development. In this thesis, adsorption and desorption of DNA on the GO surface under different buffer conditions including ionic strength, pH, and temperature were systematically evaluated. For instance, adsorption is favored in a lower pH and a higher ionic strength buffer. It was found that once a DNA was adsorbed on the surface, little desorption occurred even in low salt buffers. Even with high pH or temperature, only small percentage of adsorbed DNA can be desorbed. To completely desorb the DNA, complementary DNA is required. The energies and activation energies associated with DNA adsorption/desorption were measured and molecular pictures of these processes were obtained. With the fundamental understanding of the DNA/GO interaction, we demonstrated that it is possible to achieve sensor regeneration

without covalent immobilization. In addition, we also achieved the separation of double-stranded DNAs from single-stranded ones without using gel electrophoresis.

We also studied the fluorescence property of DNA near the GO surface using covalently attached DNA probes. It was found that the fluorophore quantum yield and lifetime changed as a function of DNA length. This study is important for rational design of covalently linked DNA sensors. This study confirmed that fluorescence quenching by GO occurs in a distance-dependent manner. Energy transfer occurred between the fluorophore and GO to result in reduced quantum yield, shorter lifetime, and lower fluorescence intensity. Although fluorescent sensors based on covalently attached DNA probes on GO have not yet been reported, the study presented here clearly supported its feasibility.

Acknowledgements

I would like to thank my thesis supervisor, Dr. Juewen Liu, for his continual encouragement and guidance. The time spent under his supervision has made research in his laboratory both a rewarding and enjoyable experience. I would like to express great thanks to my committee members, Dr. Thorsten Dieckmann and Dr. Vivek Maheshwari, for their advice and time given to evaluate my research project. I would also like to my colleagues in the lab, Neeshma Dave, Ajfan Baeissa, Marissa Wu, Brendan Smith, Nishi Bhatt, and others for making the working environment so friendly and enjoyable.

Special thanks go to my friends and family especially my parents and my sister for believing in me and for their unfailing support and love. In addition, I would also like to thank Dr. Vivek Maheshwari and Ravindra Kempaiah kindly for providing us with the samples of graphene oxide, Dr. Thorsten Dieckmann and Jason DaCosta for their assistance with the ITC experiment, Dr. Michael Palmer for allowing us use the fluorescence lifetime spectroscopy and Dr. Michaela Strüder-Kypke (Manager, Advanced Analysis Centre, University of Guelph) for her help on confocal lifetime imaging. Financial supports from the University of Waterloo and the Natural Sciences and Engineering Research Council (NSERC) of Canada in the form of research grants are greatly appreciated. Last but not least, I would use this opportunity to show my gratitude to University of Waterloo, the Department of Chemistry for financial support and for providing access to research facilities.

Dedication

I would like to dedicate this thesis to my family for their encouragement and support.

Table of Contents

List of Figures

List of Schemes

List of Abbreviations

AFM	atomic force microscopy
a.u.	arbitrary units
ATP	adenosine-5'-triphosphate
bp	base pairs
cDNA	complementary DNA
CNTs	carbon nanotubes
CVD	chemical vapor deposition
DNA	deoxyribonucleic acid
dsDNA	double-stranded DNA
EDC	1-ethyl-3-(3-dimethylaminopropyl) carbodiimide
FAM	fluorescein amidite
FETs	field effect transistors
FQM	fluorescence quenching microscopy
FRET	fluorescence resonance energy transfer
GC	gas chromatography
GC-MS	gas chromatography mass spectrometry
GO	graphene oxide
HOPG	highly ordered pyrolytic graphite
ITC	isothermal titration calorimetry
LC	liquid chromatography
LC-MS	liquid chromatography mass spectrometry
M	molar

µl	micro-liter
ml	milliliter
µm	micrometer
µM	micro-molar
MMPs	magnetic micro-particles
MS	mass spectrometry
nM	nano-molar
NIR	near-infrared
NHS	N -hydroxysuccinimide
NMR	nuclear magnetic resonance
PCR	polymerase chain reaction
PEG	polyethylene glycol
ppb	part per billion
ppm	part per million
rGO	reduced graphene oxide
RFU	relative fluorescence units
RNA	ribonucleic acid
RT-PCR	real time polymerase chain reaction
SELEX	systematic evolution of ligands by exponential enrichment
S/N	signal to noise ratio
ssDNA	single-stranded DNA
ssRNA	single-stranded RNA
UV	ultraviolet

Chapter 1: Introduction

1.1 Importance of Metabolite and Metal Ion Detection

With recent developments in metabolomics research,[1, 2] it becomes evident that the concentration of metabolites in biological fluids and tissue extracts is correlated with diseases. Compared to proteins, ribonucleic acids (RNAs), or genes, the metabolome has low molecular weight and they are higher in concentration and more stable.[3] Therefore, the quantitative measurement of metabolites can be used as an indicator for early disease diagnosis.

It is known that some metal ions are part of micronutrients that are essential for the body to produce enzymes, hormones and other substances for proper growth and development.[4] While some metal ions in a certain concentration range are beneficial for health, many others are considered very toxic. For instance, accumulation of cadmium (Cd^{2+}), mercury (Hg^{2+}), or lead (Pb^{2+}) in the body can cause neurological diseases and organ damage.[5] As a result, detection of metal ions and especially heavy metal ions is also major concern from environmental and the biological aspects. Toxic levels for some of these metals can be just above the background concentrations naturally found in the environment or food chain. Therefore, it is important to monitor the concentrations of these contaminants and take protective measures against excessive exposure.

1.2 Current Techniques for Biological and Environmental Sample Analysis

For biological and environmental samples with low complexity, they are usually analyzed by spectrophotometry or simple chromatographic separation.[1] With the improvements in analytical instrumentation over the past few decades, protocols that offer high accuracy and sensitivity for the measurement of high complexity mixtures have been well established. Methods like mass spectrometry (MS),[6] nuclear magnetic resonance spectroscopy (NMR),[7] and biosensors[8] are the common choices of analytical techniques. While MS and NMR are the principle methods for analysis, chromatographic separation and isotope labeling are usually required for more complex mixtures.[6, 8] Although MS-based methodologies provide high sensitivity for analysis, not all samples are suitable for this type of analysis. In addition, reproducibility is often the challenge for MS analysis.[3] On the other hand, NMR techniques require little or no sample preparation. However, this rapid and nondestructive analytical method usually suffers from lower sensitivity compared to MS.[9] Both NMR and MS provide qualitative and quantitative information, but the data can be quite complex sometimes.[3] The interpretation of these data usually required extensive knowledge and expertise. For metal ion detection, a number of analytical techniques that include various types of spectrometry,[10-13] voltammetry,[14-16] and chromatography[17, 18] have been developed. Although these analytical techniques provide exceptional sensitivity, many of these methods also require complicated, multi-steps sample preparation or sophisticated instrumentations. In particular, it is very difficult to achieve on-site and real-time detection and samples usually have to collected and shipped to centralized labs for detection.

1.3 Biosensors

1.3.1 Advantages of Using Biosensors

With new advances in technology and the high demand for simple and accurate on-site analysis, development of portable sensors has recently attracted more and more interest.[19, 20] Unlike instrumentation techniques, biosensors show both fast analysis and high sensitivity. Most importantly, they can be designed into simple test kits.[21] Biosensors are widely used in the food industry for quality control and in hospitals for disease diagnosis.[22-24] Biosensors can be classified as point of care devices. For instance, glucose sensors have revolutionized the health care of diabetic patients.[25] They offer moderately accurate results within a short period of time. These kinds of devices have the capability of analyzing small clinical samples at home or in hospitals.

1.3.2 Advantage of Using Aptamers for Target Recognition

Biosensor can be deconstructed into two major components: target recognition element and signal transduction element. The recognition part tends to have high affinity & specificity toward the desired targets. They are either biological or chemical entities.[26] Antibodies and enzymes are among the most commonly used molecules in making biosensors. However, it is sometimes difficult to find appropriate enzymes to cover all the important metabolites. Because of the size difference, developing antibody-based assays for small molecules is quite challenging. In addition, problems associated with enzyme or antibody immobilization and their relatively high cost and low stability have limited their applications.[27] Aptamers have recently emerged as a promising alternative. Aptamers are

single-stranded nucleic acids with 15-100 bases that can fold into a well-defined three-dimensional structure to form selective binding pockets. Most aptamers are isolated through a technique called systematic evolution of ligands by exponential enrichment (SELEX).[28-30]

Traditionally, nucleic acids are thought of as data storage molecules. They store and transfer genetic information for protein expression. Before aptamers were discovered, nucleic acids were exploited as molecular recognition elements to detect DNA and RNA targets through Watson-Crick interactions.[31] Since early 1990s, scientists have isolated aptamers and started using them as sensors for detecting non-nucleic acid targets.[28, 29] The development of aptamer technology considerably broadens the utility of nucleic acids as molecular recognition elements, because it allows the creation of DNA and RNA molecules for binding variety of analytes with high affinity and specificity.[32]

Although aptamers are different from antibodies, they mimic properties of antibodies in a variety of diagnostic formats. What makes aptamers more appealing is that they possess a number of competitive advantages over antibodies for sensing applications.[33-35] First of all, the process of antibody identification and production is time consuming and it can be very expensive especially for rare antibodies. In fact, antibodies cannot be obtained for molecules with poor immunogenicity or targets with high toxicity due to the *in vivo* selection process. Unlike antibodies, aptamers are isolated *in vitro*. Thus, they can be selected to bind essentially any target of choice.[34] Secondly, antibodies usually function at physiological conditions and are sensitive to temperature that can cause irreversible denaturation. Furthermore, the performance of the same antibody tends to vary from batch-to-batch and have a limited shelf life. Selection conditions can be manipulated

to obtain aptamers with desirable properties for analysis. Since aptamers are produced by chemical synthesis with high accuracy and reproducibility, little or no batch-to batch variation is observed.[33] Contrary to what antibodies have to offer, aptamers cannot only undergo reversible denaturation but also are stable for long-term storage.[33] Besides the ease of modification and immobilization, aptamers have sensitivity and selectivity that rival antibodies. Even though aptamers are superior to antibodies in many aspects, aptamer-based sensors are rarely seen on the market due to well-established antibody-based sensors. Because of their useful properties, aptamers are perfect choices for constructing biosensors.

1.3.3 Advantage of Using Fluorophores for Signal Generation

The signal transduction component in the biosensor usually requires high signal to noise (S/N) ratio. These signals can be generated either from electrochemical,[36-40] mass sensitive or optical methods.[41-44] Among these various optical signal transduction methods, fluorescence has been most often used due to its high sensitivity. Unlike others, fluorescence can be easily detected with simple instrument. In addition, the real-time interaction between aptamer and target can be easily detected without the separation of bound and unbound species. Since fluorophore can be easily added on aptamer, the need of target labeling is eliminated. Thus, this technique can be easily applied to any aptamer-target pair. Moreover, the availability of a large selection of fluorophores and quenchers makes it a popular choice.[45] Because different fluorophores have different excitation and emission wavelength, multiplex assays becomes feasible.

1.4 Design Strategies for DNA Aptamer Fluorescence Signal Generation

Since aptamers can be readily modified with fluorescence tags, different approaches have been focused on how to generate fluorescence labeled aptamers and how to detect fluorescence signal changes in response to aptamer binding to its target. Current designs for fluorescence signal generation are often based on target-induced conformational change of the aptamer.[45-47] These rational designs can be illustrated in Figure 1.1.

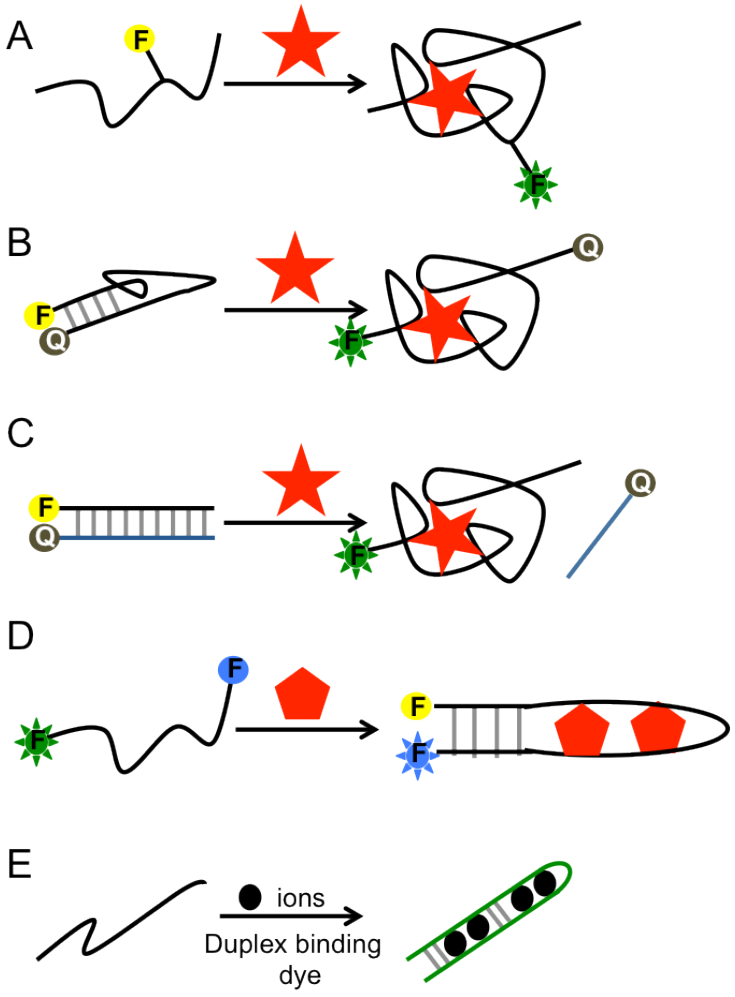

Figure 1.1 Rational design strategies for signaling aptamer. (A) Monochroomophore approach. (B), (C), & (D) Bischromophore approach with quenching mechanism. (D) Dye-staining approach.

For monochromophore approach (Figure 1A), the change of aptamer structure upon target binding will alter the electronic environment of the attached fluorophore. For the fluorophore that is sensitive to the local structure changes, this alteration leads to change in fluorescence intensity. For bischromophore approach, the arrangement of the fluorophore and quencher in the aptamer was designed in such a way that binding of the target to the aptamer will cause the separation or detachment of the quencher from the fluorophore (Figure 1.1B & C). With the increase distance between fluorophore and quencher, the efficiency of fluorescence quenching decreases. Hence, fluorescence enhancement is observed. Unlike most of the assays that require covalent fluorophore labeling, another unique way to generate aptamer fluorescence signal will require duplex binding dye (Figure 1.1D). The dye exhibits minimal fluorescence when free in solution but its fluorescence will increase up to 1,000 fold when bound to double-stranded DNA (dsDNA). For instance, SYBR Green I dye is one of the most sensitive fluorescent stains available for detecting dsDNA. The dye is commonly used in real-time polymerase chain reaction (RT-PCR) for monitoring DNA amplification. This characteristic of the dye allows for simplified assay design without the need for additional fluorescent probes.

1.5 Methods for Aptamer Immobilization

Most of the above mentioned sensors are freely dispersed in buffer, while sensor immobilization allows sensor regeneration, signal amplification, drying, patterning, and long-term storage. Aptamers immobilizations onto different substrates have been reported. Materials like gold,[48-52] glass,[51-53] silica,[54, 55] polymer[56] and magnetic beads[57-63] are common choices. The immobilization can be generally classified into three different

approaches: adsorption, covalent linkage, and affinity binding. Adsorption is the simplest immobilization method since it does not require any nucleic acid modification. Adsorption process is based on ionic, hydrophobic and Van der Waal's forces.

Unlike simple adsorption, covalent attachment to surfaces is preferred when it comes to biosensor design. Different chemical protocols for covalent attachment of aptamers to functionalized surfaces have been reported.[48, 64] Thiol and amine modified aptamers are the most popular choice. Since the strong affinity of the thiol groups for noble metal, thiol modified aptamers are commonly used to attach to gold surface to form covalent bonds (Scheme 1.2A).[48, 65, 66] Amine modified aptamer is another popular choice for covalent attachment. The aptamer is usually immobilized on to carboxylic acid coated surface (Scheme 1.1B).[67-69] This coupling reaction often uses 1-ethyl-3-(3-dimethylaminopropyl) carbodiimide (EDC) as a reagent with or without N - hydroxysuccinimide (NHS).

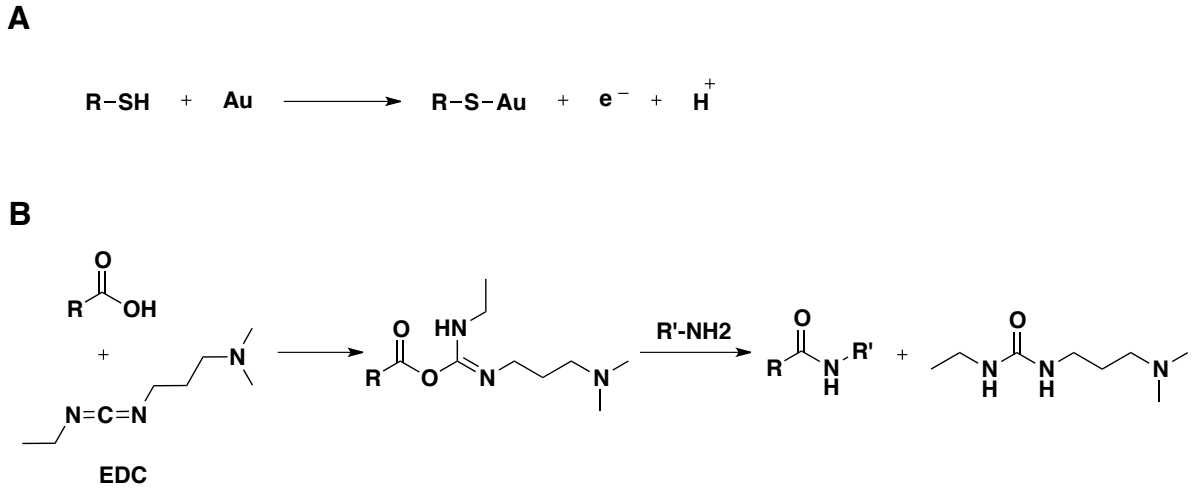

Scheme 1.1 Schematic of (A) thiol-gold bond formation & (B) Amide bond formation via reaction of carbodiimide with carboxylic acid.

Another frequently used method to immobilize the aptamer is through the strong non-covalent interaction between biotin and streptavidin ($K_D = 10^{-15}$ M).[70] Unlike other immobilization methods, binding occurs quite fast. A simple mixing and incubation at room temperature is sufficient. In addition, undesired desorption is almost unlikely due to the strong binding affinity.

1.6 Graphene and Graphene Oxide as an Aptamer Immobilization Platform

1.6.1 Graphene

Recently, graphene is also been used as immobilization platform for biosensor.[71] Graphene is a sp^2 hybridized planar carbon structure that is made up of six-atom rings in a honeycombed network with one atom thickness. This two-dimensional crystal can be considered a building block of other carbon allotropes (fullerenes, carbon nanotubes, and graphite) (Figure 1.2).[72-75]

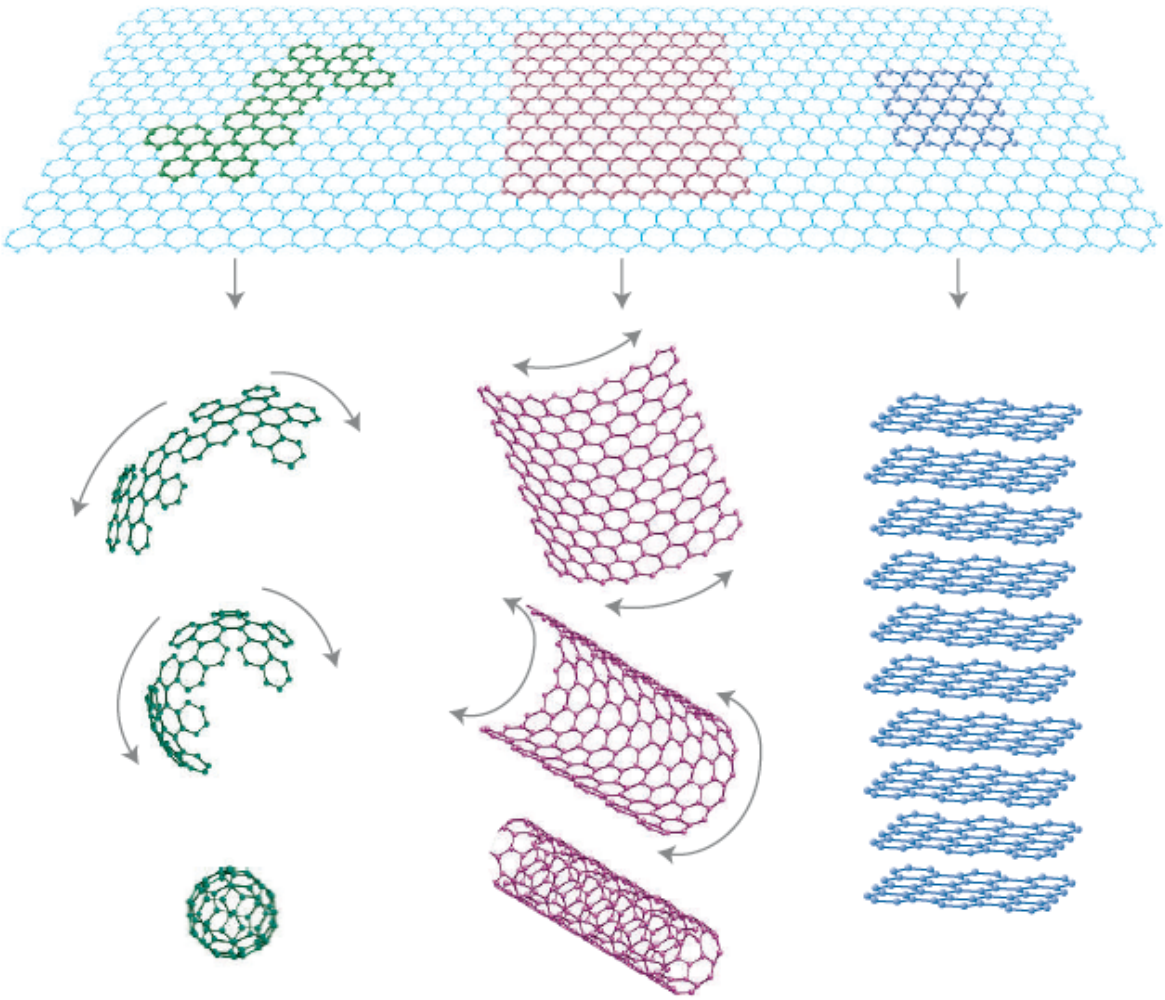

Figure 1.2 Different form of carbon allotropes. 2D graphene can form 0D fullerenes, 2D nanotubes, or 3D graphite. (reproduced with permission from ref. 73)

This single layers graphene was first isolated by Novoselov and Geim in 2004.[72] Unlike other carbon allotropes, graphene exhibits distinctly different properties.[73, 76] For instance, graphene displays a remarkable thermal conductivity, superlative structural strength, and incredible electronic flexibility.[72, 77, 78] Combination of these unique characteristics, researchers around the world are trying to use this newfound material to build batteries, solar cells, display screens, and electronic devices.[76, 77, 79]

There are different forms of graphene and their properties strongly depend on their structure (Figure 1.3). Unlike its carbon counterparts, graphene oxide (GO) contains large numbers of oxygen-containing functional groups, such as carboxyl, epoxide, and hydroxyl groups on the surfaces (Figure 1.3A & B). Since different GO preparation methods led to variability in the type and coverage of the oxygen–containing groups, different GO structures have been proposed in the past. However, the exact structure of GO is still not well known. It is only clear that majority of the oxygen-containing groups are located closely to its edges and some are located randomly in the basal plane of the sheet. GO is slightly thicker than graphene. The thickness is due to the displacement of sp^3 hybridized carbon atom above and below the plane and presence of covalently bound oxygen atoms. These polar and, in some cases, ionizable groups make GO surface extremely hydrophilic. Thus, it can be easily dispersed into single sheets in water or polar organic solvents.

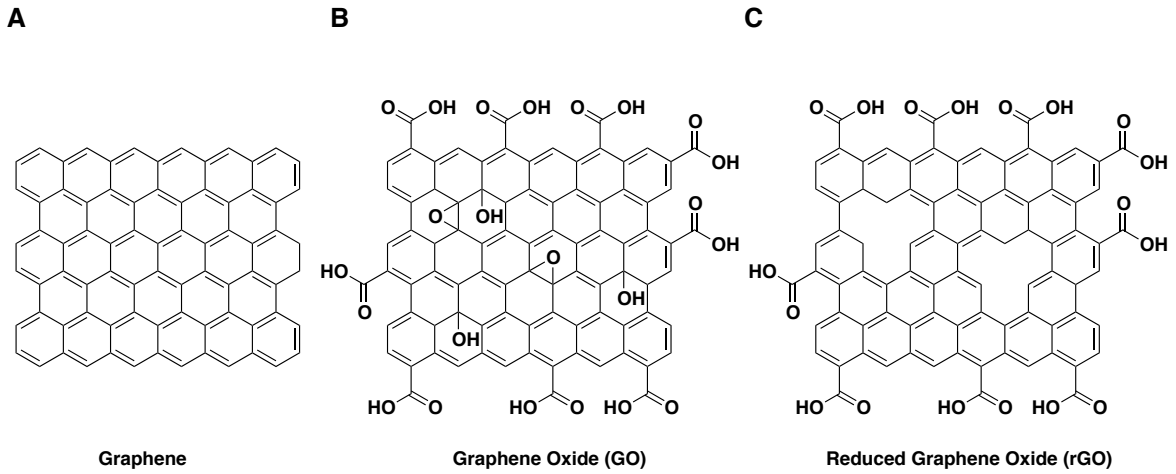

Figure 1.3 Chemical structure differences between (A) graphene, (B) graphene oxide (GO), and (C) reduced graphene oxide (rGO).

In addition, the presence of ionic groups and aromatic domains suggests that GO can interact with biomolecules in a number of ways. Although majority of the oxygen-

containing groups on the basal plane can be removed by reduction, the process usually causes some defects on the surface. These chemically reduced graphene are referred to as reduced graphene oxide (rGO). Because of these defects and residual oxygen groups on the surface, their conductivity is better than GO but worse than graphene.

1.6.2 Synthesis of Graphene and Graphene Oxide

Currently, there are many different approaches to produce grapheme-based nanomaterials. Each method has its advantages and its limitations. One of the common techniques to isolate grapheme sheets is via mechanical exfoliation of highly oriented pyrolytic graphite (HOPG).[72] In this process, monolayer or a few layers of grapheme were peeled off repeatedly from HOPG by an adhesive tape. This simple method usually produces the best quality, least modified forms of graphene. However, it is hard and time consuming to control the layers and sizes of graphene desired. Another technique is using oxidation-exfoliation-reduction process.[80] In this method, graphite was first oxidized to form graphite oxide.[81, 82] Large quantity of GO sheets were then isolated via exfoliation. rGO can be obtained with further reduction of GO. This cost effective method provide a larger scale of fabrication. However, its final rGO is not the same as graphene. rGO usually still contains a significant amount of carbon–oxygen bonds. Other methods like epitaxial growth of graphene on silicon carbide (SiC)[83, 84] and chemical vapor deposition (CVD) of hydrocarbons on metal substrates[85-87] have been reported. Even though high quality graphene can be collected, these methods required high temperature setting and were limited by its high cost and low yields. Another approach to obtain graphene is from chemical synthesis. However, this complicate approach can only produce graphene that are

limited in size. Among these methods, mechanical exfoliation remains the most popular and successful method to produce single or few layers of graphene.

1.6.3 Advantages of using Graphene and Graphene Oxide for Biosensing

1.6.3.1 Electrical and Electrochemical Properties for Electrochemical sensors

Carbon-based electrodes are known to have advantageous properties includes wide potential windows, fairly inert electrochemistry, and good electrocatalytic activities for many redox reactions.[78] Since graphene is carbon-based materials, using it for electrochemical sensor development has been the main focus to date. For example, the conduction of electrons and holes in graphene is highly sensitive to surface condition.[78] Also, graphene shows ambipolar characteristic. Combination of these properties, it has been used to develop field effect transistors (FETs) devices. The interaction between electrode surface and molecules induced conductivity or resistance changes that can be easily detected electrically. Several studies have demonstrated that this type of electrochemical sensors can exhibit very low detection limits (ppb-ppm) for a variety of gases like CO, NO_2, and NH_3.[88] With similar principle, some other studies also reported detection of proteins,[89, 89-91] small molecules,[92-94] metal ions, [95, 96] and DNA[90, 97, 98] in nM to μM range. However, GO is an electrical insulator with its layered structure distorted by a large proportion of sp^3 C-C bonds. As a result, graphene or rGO were preferred for most of the electrochemical sensing application.

1.6.3.2 Fluorescence Properties for Optical Sensors

The number of studies that exploit the optical properties of graphene for sensing is small compared with studies that use their electrochemical or electrical properties. Even though graphene derivatives itself is fluorescence from ultraviolet (UV) to near-infrared (NIR) region,[99] it was documented that fluorescence can be quenched when fluorophores were adsorbed on the surface of graphitic carbon.[100] Since graphene and GO shares some similarity, it also can quench nearby fluorescent from dye, conjugated polymers, and quantum dots.[101] Xie et al. estimated the quenching efficiency of pristine graphene to be as large as 10^3.[102] Hence, it provides a much better signal-to-noise ratio. For instance, fluorescence quenching microscopy (FQM) technique utilized this property to significantly enhance the contrast of the image. With this universal quenching property, multiple targets detection becomes feasible.[103] Therefore, graphene and its derivatives have been used in making DNA-based fluorescence resonance energy transfer (FRET) sensors.[104]

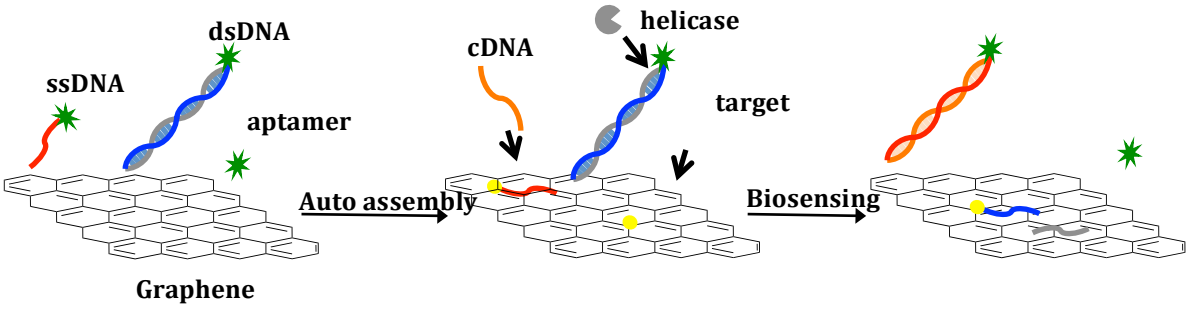

Scheme 1.2 General designs of graphene-based FRET biosensors.

In this principle design (Scheme 1.2), fluorophore-labeled ssDNA or aptamer is adsorbed

on the graphene surface and the fluorescence is quenched. On the other hand, dsDNA remains fluorescent. In the presence of cDNA or target, the binding between the ssDNA and target molecule will alter the conformation of ssDNA, and disturb the interaction between the fluorophore labeled ssDNA and graphene.[104] Once the duplex formed, the nucleobases were shielded within the negatively charges phosphate backbone. Without the π-π stacking interactions between graphene and nucleobases, the binding affinity drastically decreases. Such interactions will release the fluorophore-labeled DNA from the graphene, resulting in restoration of fluorescence.[104] In the presence of helicase, dsDNA is unwound and fluorescence labeled ssDNA and its cDNA are adsorbed on the graphene surface.[105] Just like electrochemical sensors, DNA-based optical sensors for various types of target like nucleic acids,[101, 103, 104, 106-109] proteins,[101, 105, 110, 111] virus,[112] metal ions,[103, 113, 114] and small molecules[115-119] with exceptional sensitivity have been well documented.

1.6.3.3 Other Properties

It is known that some of the potent drugs discovered are very hydrophobic and the usage is limited. Although synthesis of pro-drugs can resolve the solubility issue, efficacy of the drugs usually decreases drastically. It was discovered that GO has ability to deliver to aromatic, water insoluble molecules.[120] For example, water-insoluble aromatic drug can be attached to either polyethylene glycol (PEG) or folic acid (FA) functionalized GO to improve its solubility in physiological solutions.[120, 121] Besides, GO also has the ability to protect biomolecules from enzymatic cleavage.[122, 123] In addition, GO has an extremely large surface-to-volume ratio to interface with biomolecules. Thus, it makes GO a great material for gene transporting,[122, 124] in vivo molecular probing,[116, 122], cell imaging,[121, 125

and drug delivery.[120, 121, 126, 127] Although more studies need to be conducted before the conclusion, early publications showed low dosage of GO has no obvious toxicity compared with carbon-based nanomaterials.[76, 128] For example, GO does not have any metallic catalyst impurities that were usually found in carbon nanotubes (CNTs).[99] Unlike CNTs, dispersion of GO in aqueous does not require surfactant which sometimes has adverse effect on biocompatibility.[129] Combination of these properties, it makes graphene-based materials an ideal platform for biomedical applications.

1.7 Thesis Objective

Due to its unique properties, graphene-based nanomaterials have been employed as a solid support to be interfaced with different kinds of biomolecules. For example, nucleic acids, proteins, ions, and cells detection were well documented. In addition, several studies have focused on graphene modification and functionalization.[74, 123, 128] With proper biological modifications, graphene's biocompatibility, solubility, and selectivity can be greatly improved.[123, 128]

Even though many graphene-based biosensors have been published, the design of DNA immobilization was generally based on physiorption. Most importantly, majority of them are only focus on the detection application with little insights into the fundamental adsorption/desorption mechanisms. Although they all proven to have good sensitivity and selectivity, there are certain features still can be improved. A better understanding of the GO surface interaction with DNA will accelerate its use in applications. In my thesis work, I aimed to investigate the interaction between DNA and GO as a function of buffer

conditions. I achieved a precise molecular picture for the DNA adsorption and desorption process and measured related energies and activation energies. In addition, I also studied covalently linked DNA probes as a function of DNA length, paving the way for using covalently linked DNAs for analytical applications.

Chapter 2: DNA-Graphene Oxide Binding Characterization

2.1 Introduction

To design reliable and robust biosensors using graphene oxide and DNA, it is important to understand the interaction between these two components. Characterization of the adsorption of nucleic acid on nanostructures has previously been studied. However, these studies only involved the single nucleotides or nucleosides interactions with graphene. For those studies, various techniques like atomic force microscopy (AFM)[130] and isothermal titration calorimetry (ITC),[131] and theoretical calculation[132-134] were employed to determine the relative interaction energies. These studies showed that each nucleobase exhibits significantly different interaction strength when adsorbed on graphene. Even though the binding energies are generally small, they all found that the purine bases bind much stronger than the pyrimidines.[131, 133, 134] This result is also similar to those found with carbon nanotubes (CNTs).[130, 135-137] In addition, it was concluded that non-electrostatic interactions dominate the binding.[130] Even though adsorption of DNA on graphene and CNTs has been studied,[104, 131, 138-140] these nanostructure and GO are fundamentally different. With practical analytical applications of GO have been successfully demonstrated, in-depth studies of oligonucleotides and GO interaction have not been reported. Hence, the effect of DNA length, pH, salt, and solvent on ssDNA binding to GO was systematically evaluated. Further desorption of DNA by complementary DNA (cDNA), temperature, and the exchange of the adsorbed DNA was also studied. Such studies not only provide complementary information to understand the binding interaction between GO and DNA but also serve as a basis for further design and

optimization of GO and DNA-based biosensors.[123]

The GO synthesis and characterization were conducted by Dr. Maheshwari and his research group. The GO samples were prepared by the modified Hummers method[81, 82] and were imaged by AFM after deposition on a silicon wafer (Figure 2.1A).[141] As shown in Figure2.1B, the height of the GO sheets is ~ 1.5 nm. This confirms that they are monolayer GO and in solution they exist primarily as exfoliated single sheets. This also occurs due to oxidation of the sheets leading to a net negative charge on them. The GO prepared by this method has ~15% crystalline graphene regions on the sheet with the remaining 85% being amorphous carbon like.[142] The size of the GO sheet ranges from several tens of nanometer to several micrometers.

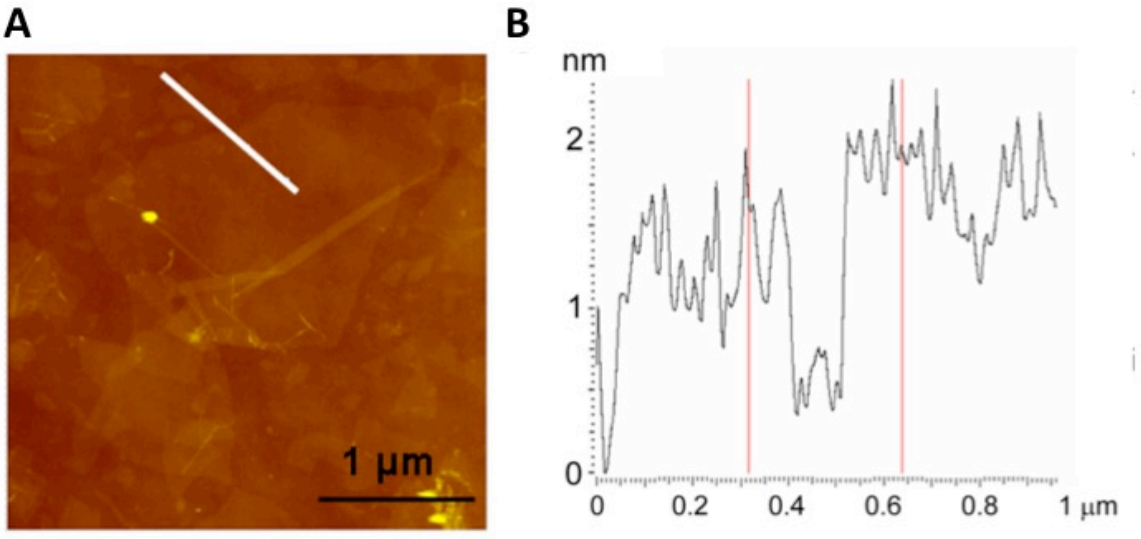

Figure 2.1 Characterizations of GO. (A) An AFM image showing GO sheets deposited on a silicon wafer. (B) The height profile of the line in (B) shows the sheet to be ~ 1.5nm in thickness.[141]

To ensure the design system has high signal to noise ratio (S/N), fluorescence was

quickly measured by fluorometer. When 100 nM FAM-labeled ssDNA was excited at 485 nm, a strong FAM emission at 520 nm was observed (Figure 2.2, solid line). Upon addition of GO, the fluorescence was greatly reduced to the baseline level (dash line).

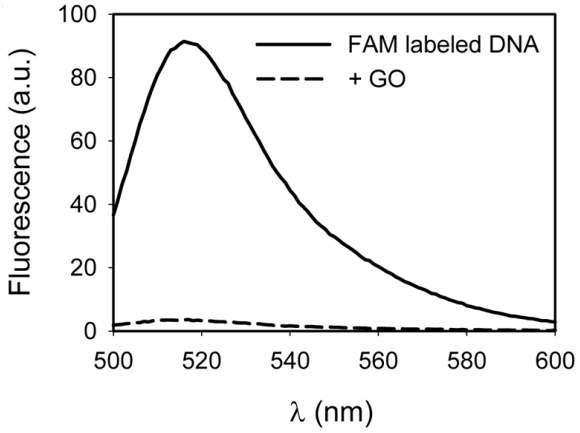

Figure 2.2 Fluorescence spectra of 100nM FAM labeled DNA in the absence and presence of 50 μg/ml GO. Both samples were dispersed in buffer containing 100 mM NaCl, 25 mM HEPES & 5 mM $MgCl_2$.

The result showed ~20 fold intensity difference which is consistent with previous findings.[103, 116] With enough of fluorescence difference, the effect of DNA/GO interaction under different conditions can be easily detected. The scheme of this whole process is shown in Scheme 2.1. To understand the adsorption DNA on GO as a function of solution condition, cations, pH, and organic solvent were used to study the effect. Once the adsorption is complete, cDNA or unmodified DNA with same sequence were added to promote DNA desorption. In addition, temperature effect on desorption was also studied.

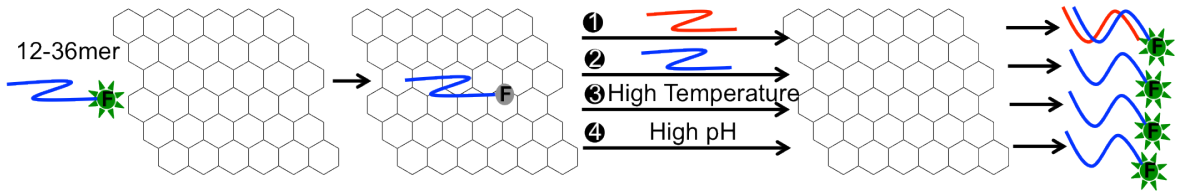

Scheme 2.1 Schematic presentation of FAM-labeled DNA adsorption and desorption on GO. Fluorescence is quenched upon adsorption. Desorption can be achieved via cDNA induced desorption (reaction 1), same DNA exchange (reaction 2), temperature induced desorption (reaction 3), or pH induced desorption (reaction 4). Noted that the aromatic rings and oxygen-contraining groups on GO are not drawn for the clarity of the figure.

To have a general idea of the binding interaction between DNA and GO, different techniques were employed. For example, fluorescence plate reader was used to monitor the reaction kinetic. Understanding reaction kinetics can provide important mechanistic insights into the surface reaction process. Moreover, the strength of the binding between DNA and GO was also studied. To evaluate the binding energy between ssDNA and GO, ITC technique was used. Thermodynamic measurement is taking place in the transition state where hydrogen bonds, van der Waals (or London dispersion) interactions and hydrophobic interactions are formed or broken.[143] ITC provide a directly approach to determine the thermodynamic characterization of the bio-molecular interactions at equilibrium state. The schematic diagram of commercially available ITC instrument is illustrated in Figure 2.3.

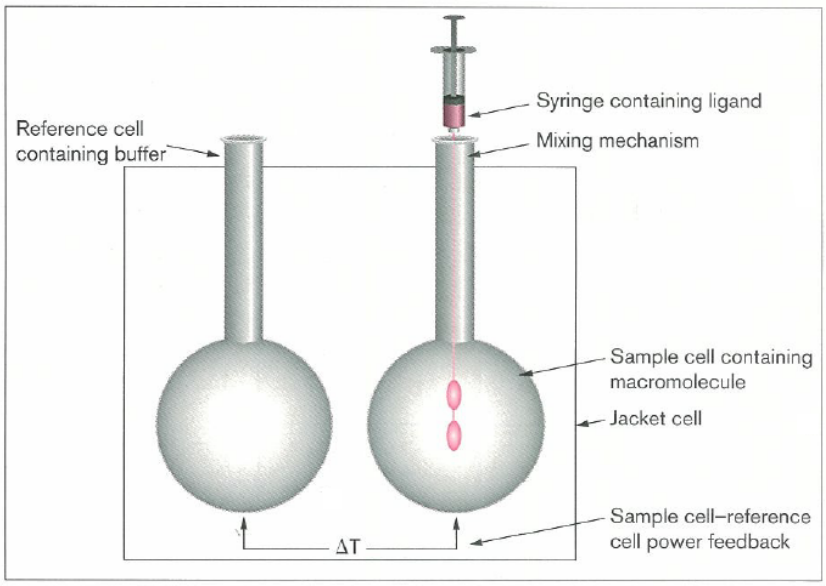

Figure 2.3 Schematic diagram of a ITC instrument. (reproduced with permission from ref. 143)

In this system, both reference and sample cells are kept at thermal equilibrium ($\Delta T = 0$). Reference cell is usually filled with water or buffer and sample cell is filled with one of the two components. When the second component is injected into the sample cell, the change in heat energy per unit time ($\mu cal\ s^{-1}$ or μW) to maintain the thermal equilibrium is measured and thermodynamic parameters can be determined subsequently. With some of these unique characteristics of DNA/GO interaction, several potential useful applications were proposed at the end of this chapter.

2.2 Results and Discussion

2.2.1 Binding Capacity

Since GO can almost quantitatively quench fluorescence, the amount of adsorbed DNA can be calculated by measuring the solution fluorescence. The overall fluorescence

quenching efficiency is equal to the percentage of DNA adsorbed and these two parameters can be used interchangeably. For adsorption studies, it is crucial to determine the surface capacity of the GO. The binding capacity can be estimated from the adsorption isotherm plot. The adsorption isotherm can be described as the partition of DNA between the solvent phase and the solid phase. To estimate the binding capacity, two fluorescence measurements were taken. The fluorescence of different amount of FAM-labeled ssDNA was first measured before overnight incubation with 20 μg/ml GO. Any unbound ssDNAs were then separated from GO sample by centrifugation. The supernatant was collected for the second fluorescence measurement. By subtracting the supernatant fluorescence from the free DNA fluorescence, an estimate amount of DNA on GO surface can be determined. As shown in Figure 2.4, at low DNA concentration (e.g. below 200 nM), the adsorption was close to quantitative. Further increase of the DNA resulted in incomplete adsorption. The result indicated that ~250 nM of DNA can be adsorbed on the 20μg/ml GO surface after long period of incubation at 25° C. It also suggested that there might be high binding affinity regions and low affinity ones. Binding of DNA in high affinity regions was irreversible with a high binding energy, while the binding energy at low affinity sites was low and an equilibrium between adsorption and desorption may be established in those regions. We can further deduce that the area ratio of the high to low binding affinity regions should be close to 200:50 or 4:1.

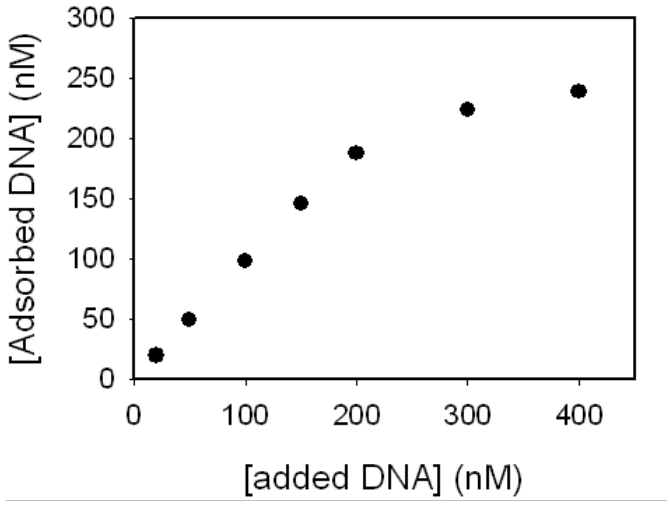

Figure 2.4 Adsorption isotherms of 27-mer DNA on GO at 25°C. Sample was incubated overnight in pH 7.6 buffer containing 150 mM NaCl, 25 mM HEPES, and 1mM $MgCl_2$.

2.2.1.1 Effect of DNA Length on Binding Capacity

Since the GO surface is limited, the binding capacity can also be affected by the length of the DNA. Four FAM-labeled ssDNAs with DNA lengths of 12, 18, 24, and 36-mer were selected. To ensure the adsorption efficiency is strictly due to the length difference, none of the sequences used here can form highly stable secondary structures under experimental conditions. As expected, binding capacity was lower when the length of DNA increased (Figure 2.5). The trend was more noticeable when the adsorption was carried out under low salt condition.

2.2.2 Effect of Salt

Many reports suggested that DNA bases contain aromatic and hydrophobic rings

that can bind to GO through hydrophobic interactions and π-π stacking.[132-134] However, the quenching efficiency was less than 30% for all the four DNA lengths in water (Figure 2.5A). This showed that the adsorption was quite ineffective in a low salt buffer. Since DNA is a polyanion and the surface of GO contains carboxylic acid groups that are deprotonated at neutral pH, electrostatic repulsion of DNA due to the negatively charged GO surface was expected. To facilitate DNA/GO short-range interaction, electrolytes are needed to screen the long-range electrostatic repulsion and bring DNA close to the GO surface for binding.

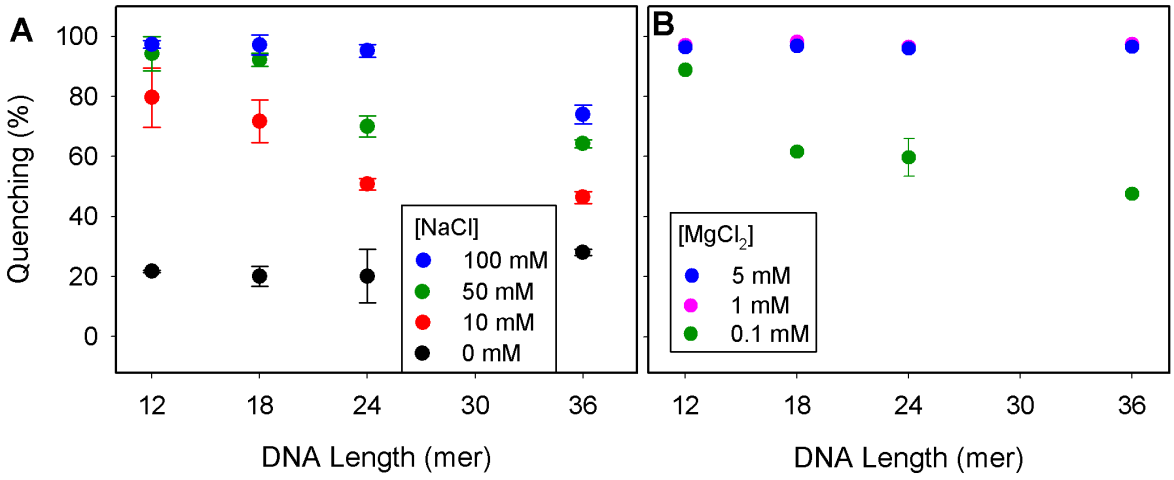

Figure 2.5 Quenching efficiency as a function of DNA length in the presence of varying concentration of NaCl (A) or $MgCl_2$ (B). The DNA concentration for GO and DNA were 170μg/ml and 1uM, respectively.[141]

Significant improvement of quenching was observed when the NaCl concentration was increased to 10 mM. At higher salt concentrations, the quenching efficiencies were progressively better. For example, the quenching was close to 100% for the three short DNAs in the presence of 100mM NaCl. Figure 2.5A also showed that the quenching efficiency for the longer DNAs was lower, suggesting weaker binding or slower

adsorption. This may result from the structure of GO that is reported as being composed of intact crystalline regions where hydrophobic interactions with DNA dominate and defective amorphous regions (oxidized) that contain the anionic functionalization which repel the DNA.[144] The size of both the domains is on the scale of 5-8 nm.[144] The 36-mer DNA has a radius of gyration of ~5 nm,[145] close to the domain size in GO and hence its adsorption is likely to be limited by the repulsive interaction with the amorphous region. Alternatively, longer DNAs may form secondary structures to shield the DNA bases to reduce the adsorption rate. Similar length dependent DNA binding to inorganic surfaces has also been observed for gold nanoparticles, where short DNAs were also more effective in binding and stabilizing colloidal gold.[146-148]

The effect of divalent Mg^{2+} ions on binding interaction is also tested. It was studied that divalent metal ions act as a bridge to connect two negatively charged molecules.[149] In comparison to monovalent ions, divalent ions should have better efficacy. As shown in Figure 2.5B, the quenching efficiencies were close to 100% for all the sequences with Mg^{2+} concentration higher than 1mM. The high quenching efficiency in Mg^{2+} can be explained by phosphate/Mg^{2+} ratio. Since the DNA concentrations used in all the experiments were 1 μM, the concentrations of phosphate linkages ranged from 11 to 35 μM. Thus, for 100 μM Mg^{2+} concentration, the number of phosphate and Mg^{2+} became comparable. As shown in Figure 2.5B, 100 μM Mg^{2+} induced ~90% quenching for the 12-mer DNA. For the 36-mer DNA, the quenching was close to 50%. This confirms a very high affinity of binding between Mg^{2+} and the DNA phosphate to allow almost quantitative interaction (e.g. the K_d between Mg^{2+} and DNA was determined to be ~0.6 μM.[150]).

2.2.2.1 Adsorption Kinetics

To further understand the salt effect on DNA/GO interaction, DNA adsorption kinetics as a function of salt was studied. Similar to the steady-state experiment, a FAM-labeled ssDNA was mixed with GO in the 5mM HEPES buffer (pH 7.6) that also contain of varying concentration of $MgCl_2$. As shown in Figure 2.6A, effective quenching was only observed when Mg^{2+} concentration was higher than 1 mM. When there was no Mg^{2+} presence in the buffer, minimum adsorption occurred. In fact, the fluorescence of the Mg^{2+} free sample did not change much even after overnight incubation. The result suggested that the presence of an adsorption activation energy barrier is related to electrostatic repulsion. In a low salt buffer, the Debye length is large (e.g. ~ 6 nm in 2.5 mM Na^+ from the HEPES buffer) and the repulsive energy is high. As a result, the thermal energy of DNA cannot cross the barrier. With a high salt concentration, the repulsion between DNA and GO was reduced to lower the energy barrier. Once the DNA is close enough to the surface, short-ranged hydrophobic interaction started to dominate and electrostatic repulsion became relatively small (vide infra).

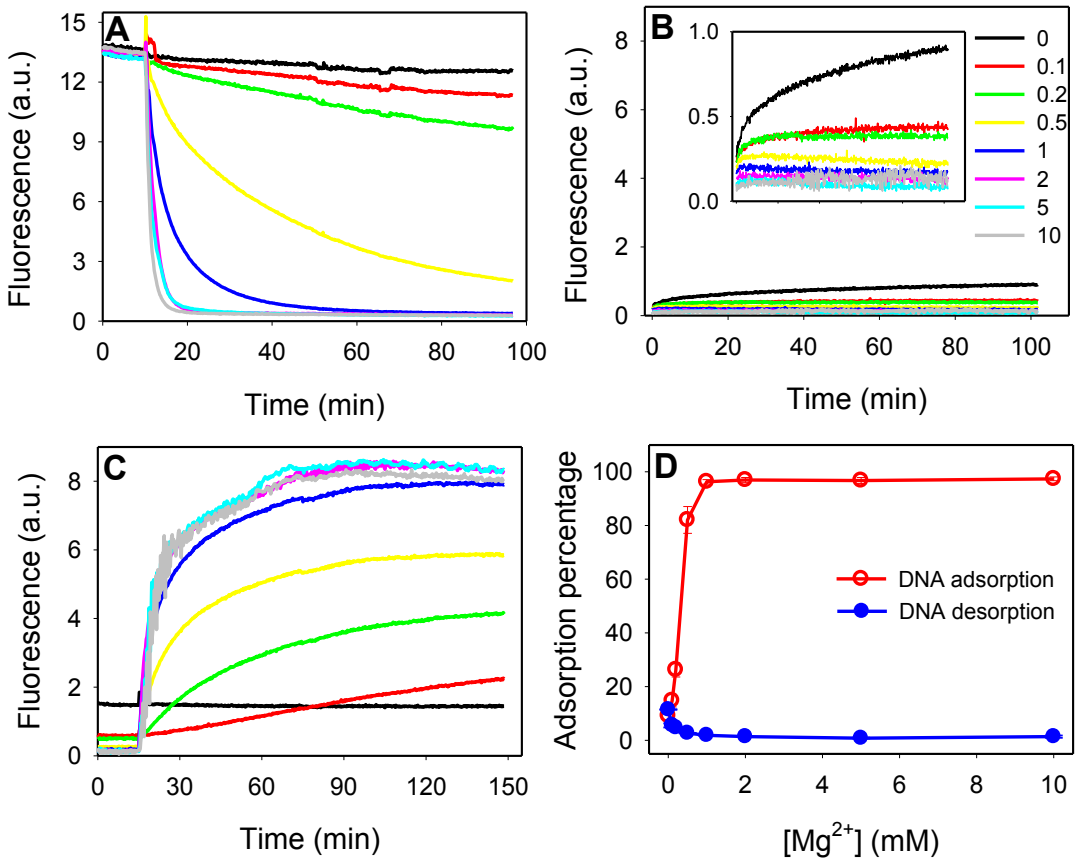

Figure 2.6 Kinetics of DNA adsorption (A) and desorption (B) in the presence of varying Mg^{2+} concentrations. Inset of (B): the same plot at a smaller y-axis scale. (C) Kinetics of DNA desorption induced by adding the cDNA in the presence of varing Mg^{2+}. (D) Percentage of DNA adsorbed and desorbed after overnight reaction as a function of Mg^{2+}. Noted that the legend in (B) is the Mg^{2+} concentration in mM and this legend is shared with (A) and (C).

2.2.2.2 Kinetic Study on Desorption

To have an overall idea of the salt effect on the DNA binding/leaving process, desorption kinetic was also studied. In this case, DNA/GO complex was first prepared in a high salt buffer to maximize the binding efficiency. Any loosely bound DNA was then washed away with water and the complex was dispersed in buffers containing varying

concentrations of Mg^{2+}. Interesting, it appeared that all samples had very low overall desorption (Figure 2.6B). Even though the effect appeared to be minimum, desorption kinetic was also depended on salt concentration. In the absence of Mg^{2+}, desorption was the highest. However, it only need 0.1 mM Mg^{2+} to effectively inhibit desorption.

It is known that adsorbed ssDNA can be desorbed by the addition of cDNA.[104] Thus, the samples were incubated with the cDNA to induce further desorption. As shown in Figure 2.6C, effective desorption was observed if Mg^{2+} was greater than 1 mM. The kinetic experiment indicated that salt was essential to overcome the repulsive barrier. These results also confirm that hydrophobic interactions are extremely important for the adsorption of ssDNA on GO. Once the dsDNA form, the bases are buried inside the helical structure and only the negatively charged phosphate groups are exposed. The disruption of hydrophobic interactions likely to cause desorption. Once the ssDNA was adsorbed, most of them remained on the surface even if the medium was switched from high salt buffer to water. The percentage of DNA adsorbed/desorbed as a function of Mg^{2+} is plotted in Figure 2.6D. For all the conditions where adsorption can effectively take place, a large desorption hysteresis is present.

2.2.3 Desorption by cDNA and DNA Exchange Comparison

To understand the effect and the importance of non-specific desorption, cDNA induced desorption and DNA exchange experiments were studied and compared. With the addition of cDNA, a fast fluorescence increase was observed (Figure 2.7A). As expected, higher concentration of the cDNA gave faster desorption kinetics. In the absence of the

cDNA, the fluorescence intensity remained low. Within the first 30 minute, ~70% of DNA on the surface was desorbed. To achieve complete desorption, sufficient time was needed. When the mixture was incubated overnight, the final fluorescence intensity reached a value close to the dsDNA sample without GO (difference within 5%).

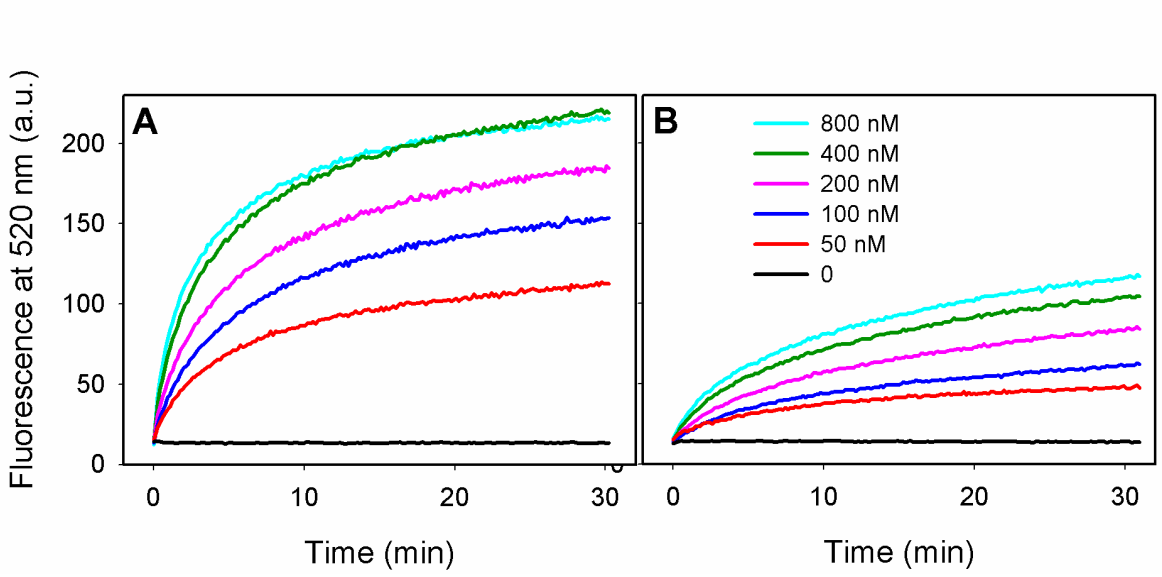

Figure 2.7 Kinetics of cDNA induced desorption or DNA/FAM-DNA exchange from GO surface. Desorption induced by adding the cDNA (A) or the same DNA but without the FAM label (B). Noted that the legend in (B) is shared with (A).

Since the DNA/GO interaction is based on adsorption, any disturbance in the system is likely to cause desorption. For instance, exchange between DNA on the surface and DNA in the solution can occur. This could be problematic when it comes to sensor design. To understand the effect of the exchange, the exchange of adsorbed DNA with free DNA in solution was also studied. Various concentrations of the unlabeled DNA with same sequence were added. As shown in Figure 2.7B, DNA concentration dependent desorption was also observed. Noted that the cDNA induced desorption kinetics were

much faster and the signals were much higher than the exchange kinetics under same condition.

Since no desorption was observed when 0 nM DNA was added, the exchange process is likely to take place through first adsorption of the non-labeled DNA followed by desorption of the labeled one. This desorption is most likely due to electrostatic repulsion between two DNAs. This observation above raised a concern on the reliability and reproducibility of this type of sensor. While a high loading of fluorophore-labeled DNA probes may allow a higher sensitivity, the exchange of adsorbed DNA by non-target DNA may generate false positive signals. To effectively detect target DNA with high specificity, free surface binding sites should exist to accommodate additional DNA.

2.2.4 ssDNA and dsDNA Adsorption Kinetic Comparison

This non-covalent bound DNA/GO sensor system is based on the assumption that dsDNA will permanently leave the surface once it is form. Although ssDNA has significantly higher binding affinity toward GO then dsDNA,[151] dsDNA still could be loosely adsorbed on GO surface. The re-adsorption especially noticeable when kinetic was monitored for a long period of time (high concentration in Figure 2.6C). This observation led us to compare the adsorption kinetics between ssDNA and dsDNA (Figure 2.8). As expected, ssDNA adsorption occurred very fast especially with 1 mM $MgCl_2$ presence in the buffer. However, a slow decrease in fluorescence for dsDNA sample also can be observed. This study confirmed that even though the dsDNA/GO binding affinity is not as strong as ssDNA/GO, the slow adsorption still could cause a certain degree of fluorescence

quenching. Thus, the reproducibility could be challenging in sensitivity experiment if the timing of the measurement is not controlled properly.

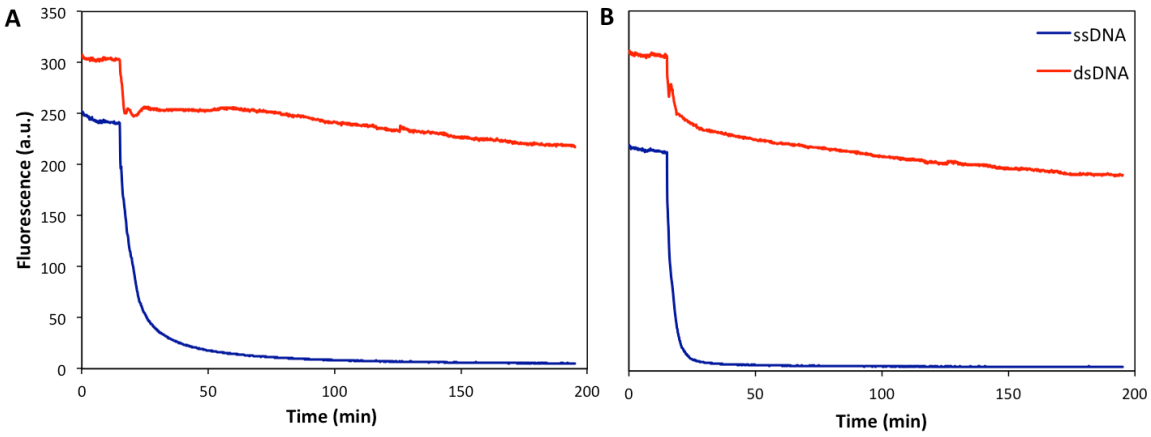

Figure 2.8 Adsorption kinetic comparisons between ssDNA and dsDNA. Samples in buffer contains 0mM $MgCl_2$ (A) and 1mM $MgCl_2$ (B).

2.2.5 Effect of pH on DNA-GO Interaction

The adsorption experiment demonstrated that electrostatic interactions play a crucial role in binding efficiency between DNA and GO. Besides tuning ionic strength, changing solution pH is another practical way to control surface charge. GO was proposed to contain several types of carboxylic acid groups that bear slightly different pK_a's.[152]

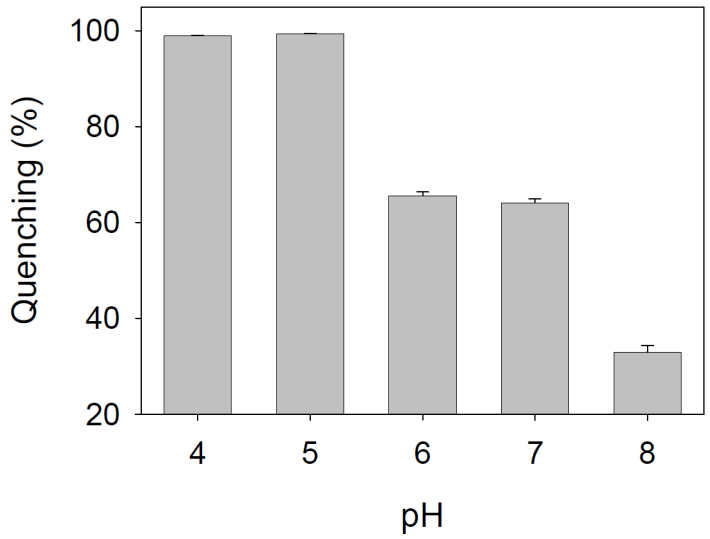

Figure 2.9 Quenching efficiency as a function of pH.

FAM is a pH-sensitive fluorophore and its quantum yield is close to zero when pH < 4. As a result, estimation of binding efficiency based on direct comparison the quenching efficiency is difficult at low pH. Therefore, the pH effect was studied indirectly. Five buffers ranging from pH 4 to 8 was prepared and the same buffers also containing 10 mM NaCl. After incubating the DNA with GO in at room temperature for an hour, the samples were centrifuged and GO was precipitated. The supernatant solution containing only the free DNA was collected and diluted with Tris-buffer (pH 8.3) before fluorescence measurement. This indirect measurement showed the binding was more effective at lower pH environment (Figure 2.9). For example, by lowering the pH from 8 to 5, the binding increased from 30% to 100%. The result indicated that tuning the solution pH could conveniently control the binding strength.

This observation can be explained by looking at the GO surface structure. The GO surface contains several different carboxylic acid groups as shown in Figure1.3B, and the

pK_a values of these groups should be close to that of benzoic acid ($pK_a = 4.2$) or acetic acid ($pK_a = 4.7$). At neutral pH, these groups are deprotonated to give a highly negatively charged surface. At close to the pK_a's, the surface charge is neutralized to reduce repulsion. While for DNA, the phosphate group has a pK_a close to zero. Therefore, the DNA backbone negative charge is always maintained in the pH range tested. On the other hand, cytosine at the N3 position has $pK_a = 4.2$ and can be protonated at pH 4. As a result, it also contributes to a reduced repulsion. In addition to the reduction of electrostatic repulsion, protonation of carboxylic acid groups on GO should also make the hydrophobic interaction stronger as the surface becomes less polar.

Based on the data of salt effect on adsorption/desorption presented earlier, the results clearly showed that sufficient DNA desorption cannot be achieved in a very low salt buffer. To effectively desorb the DNA from GO, other conditions need to be explored. The finding above seems to indicate that DNA/GO binding is less efficient in high pH environment than in low pH environment. To minimize the possibility of reducing GO at higher pH, only three buffers (5mM pH 7.5, 8.5, and 9.5) were employed to promote desorption.

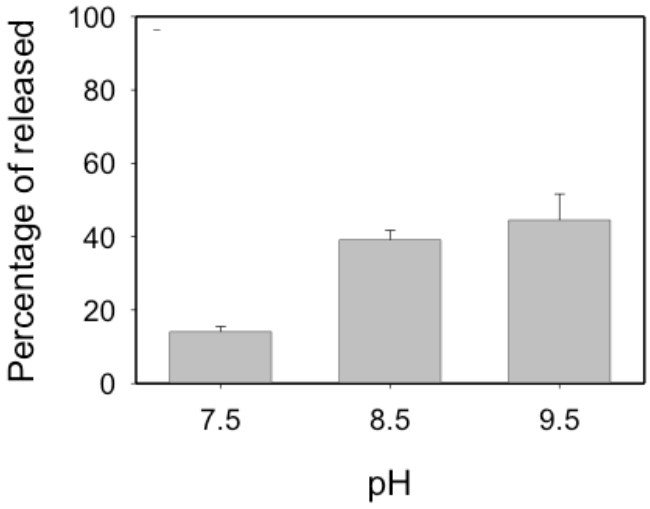

Figure 2.10 Percentage of DNA desorption after incubating in buffer of different pH after 3 hours.

As shown in Figure 2.10, sample incubated in pH 9.5 buffer showed ~50% desorption and it was the highest among all three samples. Desorption at pH 7.5 was the lowest, comparable to the 15% obtained from the previous study. While increasing pH is much more effective for desorption, it is still insufficient to achieve a complete desorption. Thereby, alternative approach like increasing temperature was planned.

2.2.6 Effect of Temperature

In addition to pH induced desorption described above, increase of temperature is also expected to facilitate desorption. Therefore, the thermal dissociation of adsorbed DNA was also studied. In this experiment, a DNA/GO complex was first dispersed in pH 7.6 buffer that contained 100 mM NaCl and 25 mM HEPES. The same DNA samples without GO were also prepared for comparison. The temperature-dependent fluorescence changes

is shown in Figure 2.11A (red curves for samples with GO and black curves for samples without GO). The fluorescence values for DNA/GO sample remained much lower compared to those of free DNAs even at 95 °C. Noted that the fluorescence decreased in free DNA was due to reduced quantum yield of the fluorophore as the temperature increased. The comparison suggests that it is quite ineffective to desorb DNA just by increasing temperature. On the other hand, this temperature insensitivity may be useful for practical applications.

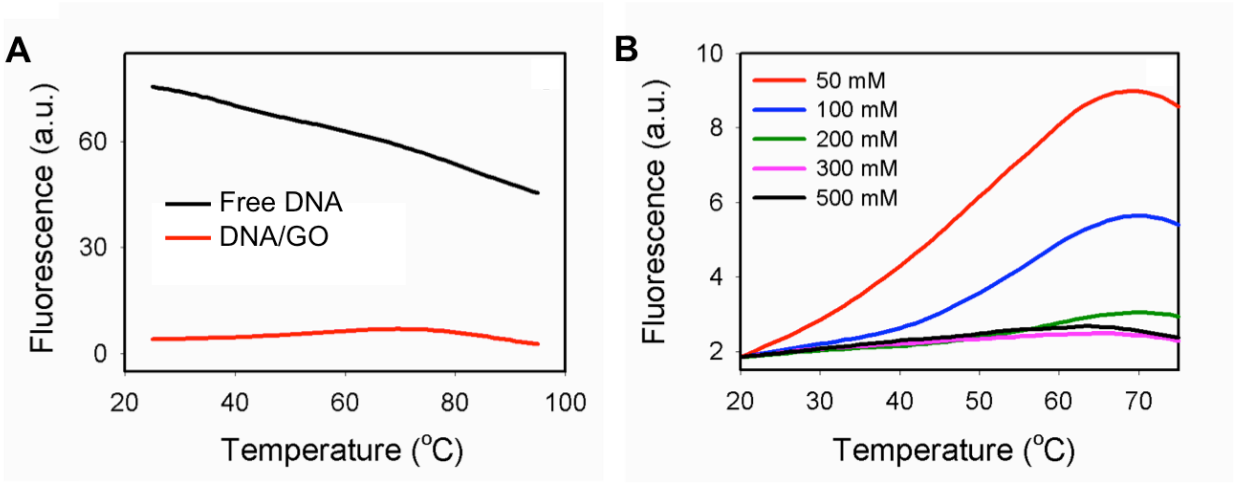

Figure 2.11 Thermal desorption of adsorbed DNA. (A) Temperature dependent fluorescence change of free DNA and DNA/GO complex in 100mM NaCl with 25mM HEPES (pH 7.6). (B) NaCl concentration dependent desorption of DNA/GO complex.

As shown in Figure 2.6B, desorption of DNA can be observed by lowering the salt buffer. Thus, the effect of NaCl concentration on the thermal dissociation of the DNA was studied (Figure 2.11B). As expected, the amount of desorbed DNA decreased with increasing salt. At concentrations higher than 200 mM NaCl, very little desorption was observed. This is consistent with the observations that higher salt leads to a stronger interaction of the DNA with GO, hence reducing thermal desorption of the absorbed DNA. Although increase in

fluorescence was observed, desorption was far from complete.

2.2.7 Combination of Temperature and pH Effect on Desorption

So far, non-specific desorption was tested under low salt, high pH, and high temperature separately. Each of this parameter has its effect to a certain degree. However, none of the above conditions can promote complete desorption of the DNA from the GO surface. This suggested that DNA/GO interaction is pretty strong. One way to overcome the desorption energy barrier is to disperse the DNA/GO complex in low salt buffer and increase the temperature and pH simultaneously. Three identical DNA/GO complexes in different pH buffer were load into a real-time PCR. Fluorescence was monitored as a function of temperature (Figure2.12).

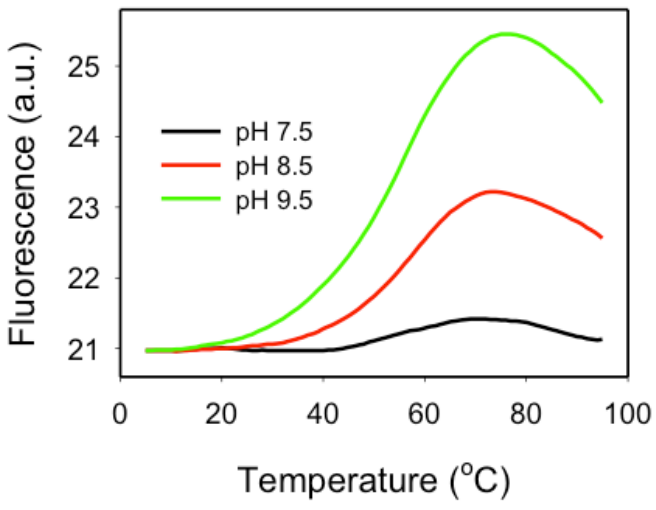

Figure 2.12 Thermal desorption of DNA at varying pH buffers (5mM)

As can be seen, increase of temperature resulted in increased fluorescence for all the three tested pH buffers. At low salt buffer, the data clearly showed that DNA desorption was favored at higher temperature. In addition, desorption was even more effective at higher pH. Consequently, a combination of high pH, low salt and high temperature appeared to be necessary to achieve effective desorption of adsorbed DNA.

2.2.8 Adsorption Activation Energy

From the above experiments, we gained a qualitative understanding about the adsorption/desorption process. The fact that a large hysteresis was present for DNA desorption suggested the presence of a high activation energy barrier. In addition, activation energy barrier also existed at low salt buffers for DNA adsorption. To estimate the height of such barriers, adsorption kinetics experiment at varying temperatures need be conducted. Previous experiments demonstrated that the salt concentration greatly affected the adsorption kinetic. If the salt concentration was too low, the adsorption reactions is too slow to obtain a good fitting. To ensure the reaction can be completed within a reasonable time frame, 25 mM HEPES (pH 7.6) with 0.1 mM Mg^{2+} was used. As expected, incubation at higher temperatures facilitated faster adsorption (Figure 2.13A).

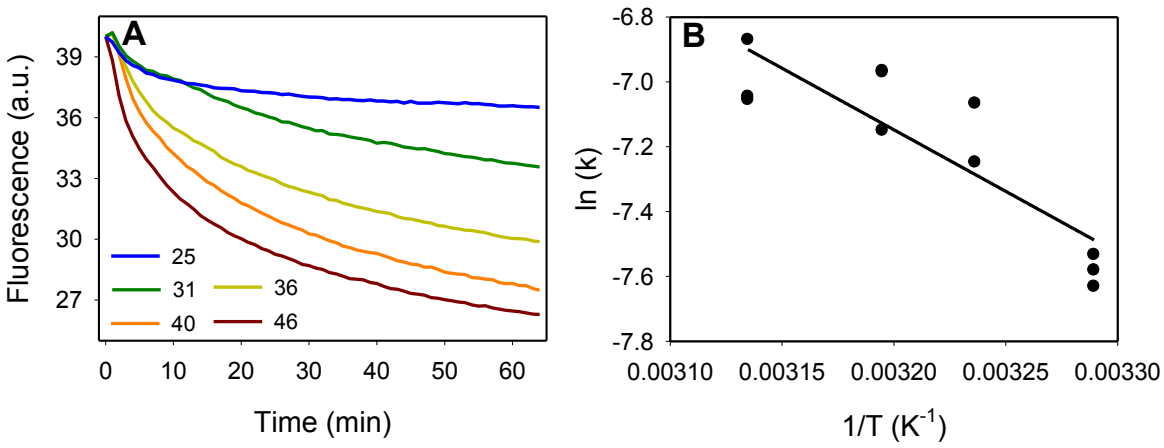

Figure 2.13 (A) Adsorption kinetics at varying temperatures. (B) The Arrhenius plot of the DNA adsorption reaction (31°C - 46°C).

The kinetic traces were then fitted to the first order reaction model and the rate constant was determined. By using Arrhenius equation (equation 2.1), activation adsorption energy can also be determined.

$$\ln(k) = \ln(A) - \frac{E_a}{RT} \tag{2.1}$$

The temperature range of 31 to 46 °C was used for this study. If the temperature was too low, the reaction was far from completion and an accurate fitting cannot be obtained. On the other hand, if the temperature was too high, desorption started to occur. Based on the previous study, very little thermal desorption was observed if temperature was lower than 46 °C for samples in pH 7.5 buffer (Figure 2.13). Under this condition, DNA adsorption can be considered to be an irreversible reaction.

The Arrhenius plot of ln(k) versus $1/T$ was shown in Figure 2.13B and the data

points were fit to a linear equation. The slope of this line is $-E_a/R$, where E_a is the adsorption activation energy and R is the gas constant. Based on this, the adsorption activation energy was calculated to be 31.6 kJ/mol. Little information on the adsorption activation energy can be found in the literature related to DNA adsorption onto a solid surface. For global proteins, E_a of 5 to 50 kJ/mol at liquid interfaces was reported.[153] In another example, the adsorption of a dehydrogenase protein on magnetic Fe_3O_4-chitosan nanoparticles had an E_a of 27.6 kJ/mol.[154] It seems like that the experimental E_a value of our DNA is comparable to the reported protein. The thermal energy of the DNA at room temperature is about 2.5 kJ/mol. Therefore, it is much lower than this measured activation energy barrier and DNA adsorption on GO at low salt buffer is an activated process. With sufficient thermal energy provided, this energy barrier can be surpassed. The barrier height should be a function of ionic strength since adsorption can be achieved at room temperature with high salt. As can be observed from Figure 2.6A, adsorption can be quite fast even at room temperature if the salt concentration was high, which further confirmed the electrostatic nature of the activation barrier.

2.2.9 Adsorption Energy and Desorption Activation Energy

As our understanding, the amount of heat released from the adsorption process should be the same as desorption activation energy. To measure the adsorption heat directly, ITC technique was employed. The titration curve is shown in Figure 2.14 and several features can be observed. First, the heat released progressively decreased with more DNA injected. A value of ΔH = 61.3 kJ/mol at pH 7.5 by measuring the heat from the first injection was determined. The amount of heat released for the second injection to

be 47.9 kJ/mol and the third to be 32.7 kJ/mol. After the third injection, the signal became very small. Based on the binding capacity that was previous estimated (Figure 2.1), saturation should occur after six injections. However, an abrupt change in the ITC trace was observed after three injections. This suggested the presence of different binding sites on the surface with different binding energy. The amount of DNA introduced in the first injections occupied the high affinity site to release more heat. The following three injections, although still can bind to GO, resulted in much lower heat release. With a closer look, the broad transition (20 to 70 °C) shown in thermal dissociation experiment also support the presence of different binding affinities (Figure 2.12).

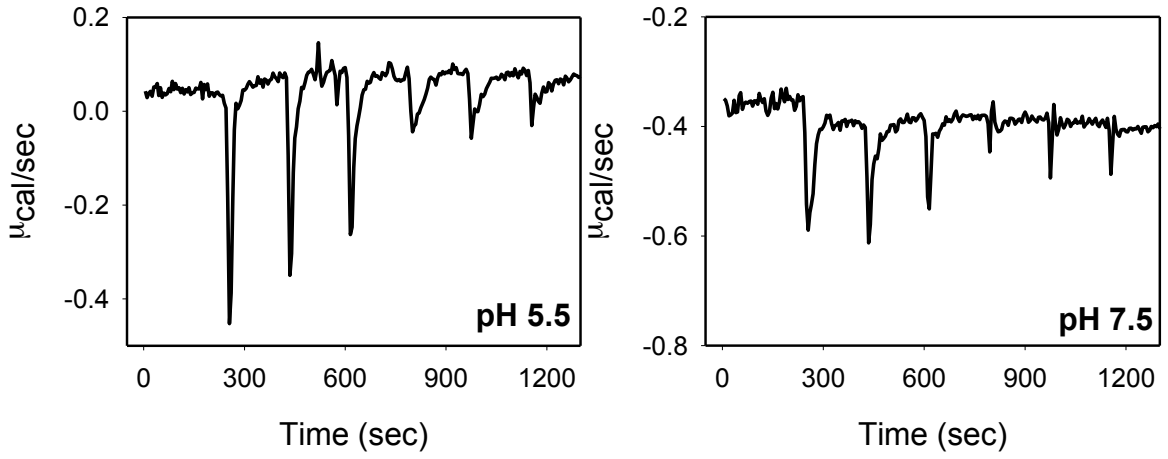

Figure 2.14 ITC trances of DNA-GO binding at pH 5.5 (A) and 7.5 (B).

It is known that lowering the pH can facilitate binding. As expected, ITC measurement at pH 5.5 showed the first three injections resulted in 89.0, 92.8, and 80.3 kJ/mol of heat. Such energy is close to chemisorption (100 kJ/mol) and that can explain the high stability of the DNA on the GO surface, especially at low pH.

To summarize our finding about the adsorption and desorption energy, a model shown in Figure 2.15 is used. In this diagram, the desorption activation energy is the sum of the adsorption energy and the adsorption activation energy, which also contributed to the difficultly associated with desorption. We measured the adsorption activation energy in a low salt buffer and the adsorption energy in a high salt buffer. The reason for the adsorption activation barrier is due to electrostatic repulsion. To favor adsorption, the activation barrier can be easily overcome by adding salt or lower pH. We have explored the buffer conditions to promote desorption and only a combination of low salt, high pH and high temperature is favorable.

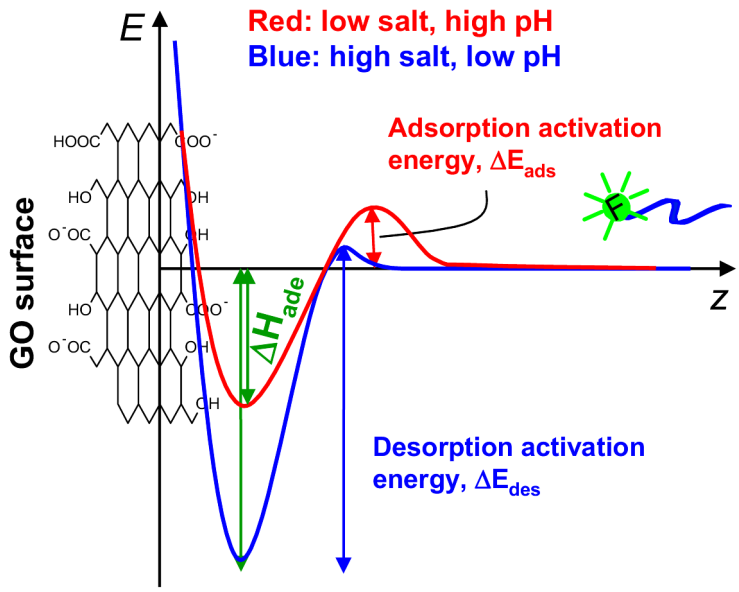

Figure 2.15 An energy diagram of DNA approaching the GO surface in an aqueous solution. Two conditions are shown. The conditions in the red curve favor desorption while adsorption shows a large activation barrier. In the blue curve, adsorption readily occurs but desorption is very difficult.

2.3 Conclusion

While practical analytical applications of graphene-based optical sensors are well

demonstrated, the fundamental understanding of binding between DNA and GO received relatively less attention. Here, we have systematically studied the adsorption and desorption of fluorescent-labeled oligonucleotides on GO surface. Initial studies indicated that high ionic strength was required to initiate the adsorption of ssDNA on GO. Once adsorbed, little desorption occurs even in low salt buffers. This finding suggested that other short ranged interactions such as hydrophobic interactions dominated the binding. However, it also posed a technical challenge in terms of removing those adsorbed ssDNA besides adding cDNA. By testing different buffer condition, we found that using a combination of low salt, high pH, and high temperature can help to achieve sufficient ssDNA desorption. We also measured the adsorption kinetics at varying temperatures to obtain the activation energy for adsorption and we used ITC to measure the adsorption energy. Overall, the DNA/GO binding is very stable. However, the binding can be easily modulated with precise control of buffer conditions.

2.4 Experimental Section

2.4.1 Chemicals

All DNA samples were purchased from Integrated DNA Technologies (Coralville, IA). The DNA sequences used in this experiments are: 12-mer, CAC TGA CCT GGG; 18-mer, CTT GAG AAA GGG CTG CCA; 24-mer, ACG CAT CTG TGA AGA GAA CCT GGG; and 36-mer, TAC CTG GGG GAG TAT TGC GGA GGA AGG TTC CAG GTA. The adenosine aptamer sequence is ACC TGG GGG AGT ATT GCG GAG GAA GGT. All the sequences are listed from the 5′ to 3′-end. Each DNA carries a FAM (6-

carboxyfluorescein) modification on the 5′- end. Sodium chloride, magnesium chloride, sodium acetate, 4-Morpholineethanesulfonate (MES), 4-(2-hydroxyethyl)piperazine-1-ethanesulfonate (HEPES), and Tris(hydroxymethyl)aminomethane (Tris) were purchased from Mandel Scientific (Guelph, Ontario, Canada). Sulfuric acid, potassium persulfate, phosphorous pentoxide, hydrogen peroxide, potassium permanganate were purchased from Sigma-Aldrich. Acetic acid and hydrochloric acid were purchased from VWR. Graphite flakes were purchased from Fisher. Millipore water was used for all the experiments.

2.4.2 Synthesis and Characterization of GO

GO was synthesized using the modified Hummers method.[81, 82] Briefly, 3 g of graphite flakes (~325 mesh size) were dissolved in 10 mL of sulfuric acid (H_2SO_4). Potassium persulfate ($K_2S_2O_8$) and phosphorous pentoxide (P_2O_5) were added to the solution as oxidizing agents and stirred at 90 °C until the flakes were dissolved. The solution was stirred at 80 °C for 4 hrs and subsequently diluted with 500 mL water. The diluted solution was stirred overnight, washed and filtered to get a dry powder. This pre-oxidized GO powder was subjected to further oxidation with 125 mL of H_2SO_4 and 15 g of $KMnO_4$ in an ice bath and stirred for 2 hrs. 130 ml of water was added to the solution causing the temperature to rise to 95 °C. After 15 minutes, 15 mL of H_2O_2 was added. Finally the solution was diluted with 400 mL water and the resultant yellow-brown suspension was stirred overnight. This GO solution was filtered and washed until it reached a neutral pH and also purified by dialysis to remove excess ions. Finally, the GO solution was suspended at a concentration of 200 μg/mL.

The synthesized GO sheets were absorbed on a silicon chip, which was pretreated with piranha and (3-Aminopropyl) triethoxysilane. The characterization was carried out a Nanoscope IV AFM Instrument (Veeco).

2.4.3 Steady-State Fluorescence Measurement

2.4.3.1 Quenching Efficiency

100nM DNA was incubated with 50 μg/ml of GO in 100 mM NaCl, 25 mM HEPES and 5mM $MgCl_2$ for ~ 1 hour. 100nM free DNA in the same buffer was also prepared. The fluorescence spectra of the two samples were then collected by using Varian Eclipse spectrofluorometer. The excitation wavelength was set at 485 nm and the emission from 500 to 600nm was collected.

2.4.3.2 GO Binding Capacity Estimation

In this experiment, 20 μg/ml of GO was incubated with various concentration of adenosine aptamer in buffer (150 mM NaCl, 25 mM HEPES, 1 mM $MgCl_2$) for overnight. Samples were then centrifuged at 15000 RPM to collect supernatants. The fluorescence of supernatant was measured with Tecan Infinite F200 Pro plate reader. DNA samples without GO were also prepared for comparison.

2.4.3.3 DNA Length and Salt Effect

Four ssDNA with length range from12-mer to 36-mer were used. In this experiment, 1μM DNA was incubated with 170 μg/ml GO in varying concentrations of salt for ~ 1 hour. Samples without GO were also prepared as corresponding references. Fluorescence was measured at 25 °C.

2.4.3.4 pH Effect

To study the pH effect, four buffer with different pH were prepared (acetate buffer: pH 4 & 5; MES: pH 6; Tris-HCl: pH 7 & 8). 1μM DNA was incubated with 170 μg/ml GO in contained 50mM buffer with 10 mM NaCl for ~ 1 hour. The samples were centrifuged at 15000 RPM for 20 min. 20 μl of the supernatant solution was then mixed with 180 μl of 100mM Tris-HCl (pH 8.3) buffer before the measurement.

2.4.4 Kinetics Study

The kinetics of adsorption and desorption was monitored by Tecan Infinite F200 Pro plate reader at 25 °C. 50 μl of sample was used for the kinetic study.

2.4.4.1 Effect of Salt

For the effect on adsorption, 20 μg/ml GO was dispersed in 5 mM HEPES (pH 7.5) with different $MgCl_2$ concentration. For the effect on desorption, 20 μg/ml GO was first

incubated with 100 nM DNA in buffer (150mM NaCl, 25 mM HEPES and 1mM $MgCl_2$) for ~ 1 hour. Samples were then centrifuged to remove supernatants and washed with small volume of water before re-suspended in 5 mM HEPES (pH 7.5) with various concentration of $MgCl_2$.

2.4.4.2 cDNA Induced Desorption and DNA Exchange

The DNA/GO complex was prepared by mixing 50 pmol of the 24-mer DNA and 20 μL of 200 μg/mL GO in 5 mM $MgCl_2$, 100 mM NaCl, and 25 mM HEPES, pH 7.6. This mixture was centrifuged to remove free DNA in the supernatant and then re-dispersed in 200 μL of the same buffer. Desorption experiment was carried out with the fluorescence plate reader. Each well contained 65 μL of the buffer with 15 μL of the DNA/GO complex solution. 20 μL of the c-DNA was then added to initiate the desorption reaction. Exchange of adsorbed DNA was studied using a similar method and the same 24-mer DNA without the fluorophore label was added.

2.4.5 Thermal Desorption

Temperature induced desorption of DNA experiment was carried out in the real-time PCR thermocycler (Bio-Rad CFX-96) using a sample volume of 20 μL. The temperature was increased every 1 °C with a holding time of 1 min before each reading. 500 nM DNA was incubated with 100 μg/mL of GO in buffer (150 mM NaCl, 25 mM HEPES and 1 mM $MgCl_2$) at room temperature for ~ 1 hours before the analysis. Samples

were then centrifuged at 15000 RPM to remove excess of DNA and washed with small volume of water. For NaCl-dependent studies, 50 mM to 500 mM of NaCl concentrations were tested. For pH-dependent studies, samples were re-dispersed in 5 mM Tris-HCl (pH 7.5, 8.5 and 9.5).

2.4.6 ITC Analysis on Adenosine Aptamer/GO Binding

For the titration measurement, 250 μL of GO is needed in the cell chamber and 40 μL of adenosine aptamer is needed in the syringe. The experiments were conducted at 25 °C. 50uM adenosine solution was titrated into 800 μg/mL GO. For pH 7.5 measurement, buffer contained 150 mM NaCl, 25 mM HEPES, and 1 mM $MgCl_2$ was used. For pH 5.5, 25 mM citrate instead of HEPES was used. The amount of released heat was measurement after each addition by using MicroCal 200.

Chapter 3. Analytical Applications of Physisorbed DNA on Graphene Oxide

3.1 Introduction

Aptamers are short single-stranded DNAs that can be selected to bind to any target of interest.[28, 29, 32, 34] Because of the advantages of using aptamers as molecular recognition elements, aptamers can be used in sensors.[34, 45] With sensor immobilization, advantages like sensor regeneration and signal amplification became possible. Recently, it was discovered that non-structured ssDNA can be strongly adsorbed on the GO surface and desorbed upon forming dsDNA or well-folded structure. Combination with large surface area and intrinsic fluorescence quenching ability, GO became an ideal platform for designing optical aptasensors. All these reports have demonstrated the good sensitivity and selectivity based on DNA/GO scaffold.[105-107, 110, 113, 128, 155] Even though these types of sensors are easy to prepare, non-covalent immobilization usually means sensor regeneration is challenging. After detection, it is difficult to re-adsorb the DNA and wash away the target molecule since there is no covalent linkage between the aptamer and the surface. If a re-adsorption mechanism can be introduced, this system can serve as a re-generable sensor.

In the previous chapter, we demonstrated that DNA binding to GO was stronger at lower pH. It is common that most of the aptamers selections were carried out at the neutral pH. Thus, it was assumed that lowering the pH might have an adverse effect on aptamer binding. Since aptamer-target and aptamer-GO have totally opposite binding efficiency at low pH environment, it was thought the reversible operation is plausible if the pH of the

system was carefully tuned. In this scheme (Scheme 3.1), mixing a fluorescently labeled aptamer with GO resulted in quenched fluorescence. Upon addition of the target molecule, the aptamer can bind to the target and desorb from the surface, resulting in fluorescence enhancement (step 1). After detection, pH of the mixture was acidified. The low pH environment prompted the dissociation of aptamer-target complex and facilitated the aptamer-GO binding (step 2). Once the reverse process is completed and the target is removed, sensor can be easily regenerated by restoring in neutral pH buffer (step 3). Besides the regeneration, this dual control system can also be used as a logic gate.

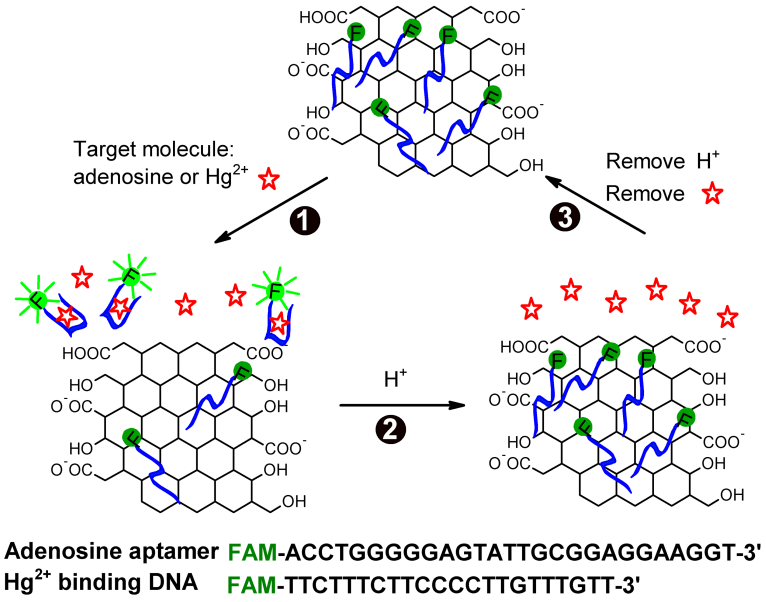

Scheme 3.1 Schematic presentations of sensor operation (step 1) and regeneration (step 2 & 3). The aromatic rings on GO are not drawn for the clarity of the figure. The aptamer sequences are listed from the 5' to 3'-end.

One of the many reasons that GO became a popular choice for aptamer-based sensor is the discovery of its excellent selective adsorption on ssDNA and dsDNA. Besides utilizing this intrinsic characteristic for the sensor application, it is also possible to use it as

ssDNA scavenger. Based on the kinetic study from previous chapter (Section 2.2.4), we knew that ssDNA adsorbed on GO surface much faster than dsDNA did. With this in mind, separating ssDNA/dsDNA mixture is feasible without the need of electrophoresis. On top of that, the separation can be achieved within a short period of time.

3.2 Results and Discussion

3.2.1 Effect of pH on Aptamer - Target Interaction

To test the pH effect on aptamer/target binding, ITC technique was employed to accurately determine the dissociation constant (K_d). At pH 7.5, we obtained a K_d of 13.1 ± 1.8 μM (Figure 3.1A), which was comparable to the literature reported 6 ± 3 μM.[156] At pH 5.5, the K_d increased slightly to ~19.6 μM (Figure 3.1B). At pH 3.5, however, no obvious binding was observed (Figure 3.1C). Only when the adenosine concentration was increased to 10 mM, did we obtain a binding curve with a K_d of 202 μM (Figure 3.1C, inset).

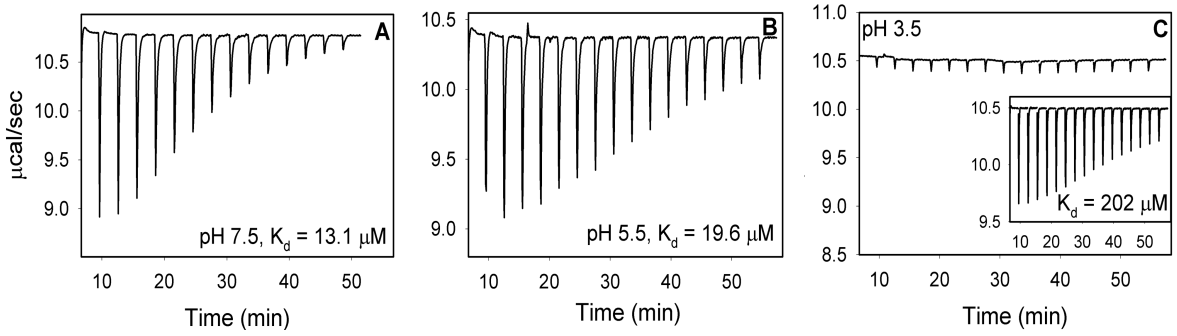

Figure 3.1 ITC traces of adenosine aptamer binding at pH 7.5 (A), 5.5 (B), and 3.5 (C).

The low binding efficiency at pH 3.5 is probably due to partial protonation of the A and C

bases in DNA and the target molecule adenosine. Consequently, it is likely to interfere with hydrogen bonding and charge interactions. This experiment supports our hypothesis that the adenosine aptamer binding is weakened at low pH. Note that similar pH effect on a cocaine aptamer binding was also recently reported.[157, 158]

3.2.2 Synergetic pH Effect on Target/Aptamer/GO Interaction

To ensure the pH and salt effect can also be duplicated on the aptamer-GO binding, FAM-labeled adenosine aptamer was used here. The adenosine sensor was prepared by incubating 500 nM FAM-labeled adenosine aptamer with 100 μg/ml GO in various buffer condition for an hour. The supernatant was then collected and the pH was adjusted accordingly before the measurement. At high ionic strength (150 mM NaCl, 25 mM HEPES, 1 mM $MgCl_2$, pH 7.6), adsorption was close to 100% at all three pH values tested (Figure 3.2, black bars). On the other hand, the aptamer showed almost no binding to GO at pH 7.5 but close to quantitative binding in lower pH and low salt buffer condition (25 mM HEPES, grey bars). This experimental finding suggested that by tuning the pH and ionic strength of the solution, the adsorption of aptamer on GO could be controlled. Importantly, the pH effect was synergistic; target/aptamer/GO binding interaction can be tuned by adjusting the pH.

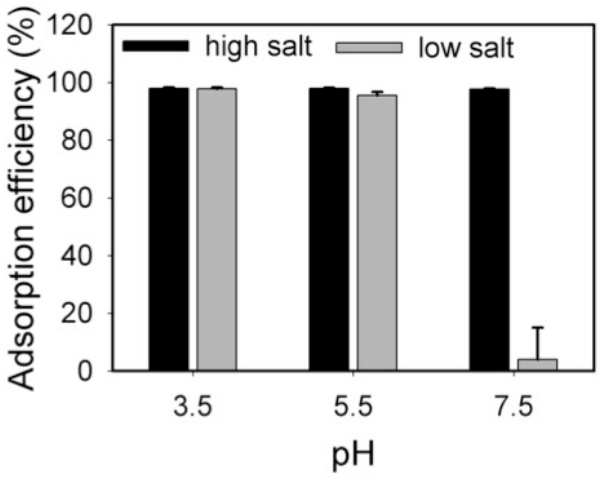

Figure 3.2 Salt and pH-dependent binding of the adenosine aptamer by GO.

3.2.3 Sensor Regeneration

To show this concept can be achieved and the generality of this approach, adenosine aptamer[156] and Hg^{2+} aptamer[159] were chosen for the demonstration. For FAM-labeled adenosine aptamer, mixing with GO resulted in low fluorescence without the presence of adenosine. 10 minute after the addition of 2 mM adenosine, fluorescence enhancement reached a plateau (Figure 3.3A, solid black curve). The sample was subsequently acidified by incubating with 500 mM citrate buffer (pH 3.5) for 40 min for regeneration. At this pH, the aptamer should release the bound adenosine and re-adsorb onto the GO surface. The sample was centrifuged and the supernatant was removed from the GO pallet. Another adenosine sensor was regenerated in pH 7.5 HEPES buffer (50 mM, grey curve) for comparison. After regeneration, both samples were re-dispersed in incubation buffer and adenosine was again added. The final fluorescence reached about half of the original value for the sample regenerated at pH 3.5 but less than 20% for the one washed at pH 7.5.

The second aptamer used here is FAM-labeled DNA that is rich in thymine and can bind with mercury ions. Because of the metal-nucleotide interaction is highly specific, a T-T base pair can only be stabilized by Hg^{2+}. Since mercury binding to the thymine base is accompanied by the release of the imino proton,[159, 160] lowering pH should reduce Hg^{2+} binding. To prevent the binding of Hg^{2+} ions with chloride and HEPES, the reaction buffer was switched to 150 mM $NaNO_3$, 5 mM Tris nitrate, pH 8.0. Like the previous adenosine example, the fold of fluorescence increase for samples regenerated at pH 3.5 was also much higher than those regenerated at pH 7.5 (Figure 3.3B).

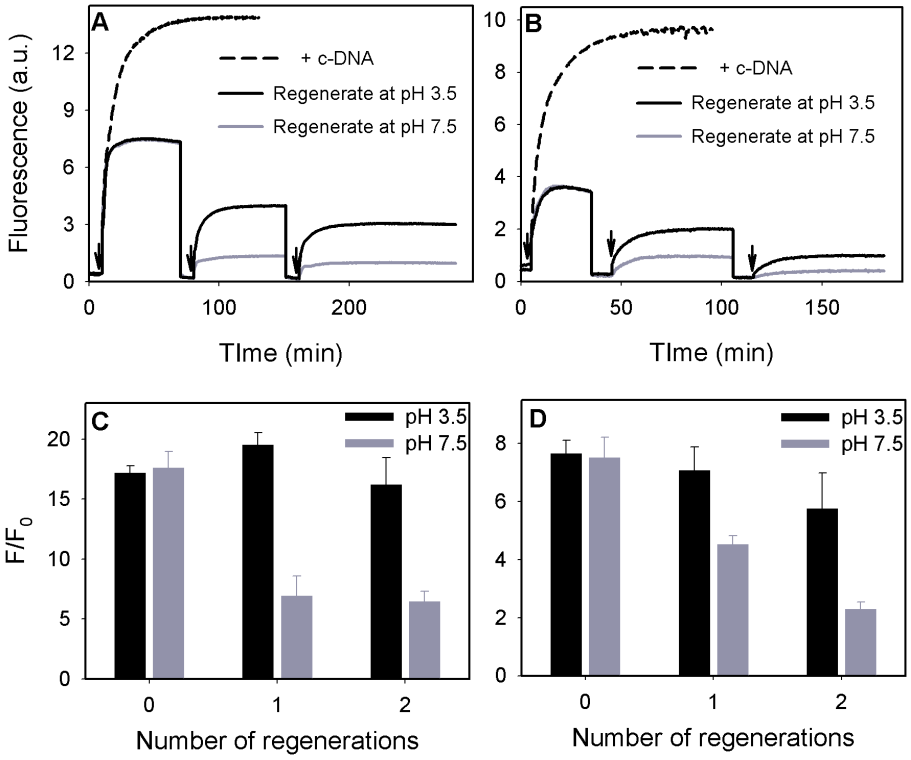

Figure 3.3 Sensor regeneration. Kinetics of fluorescence change for the adenosine (A) and Hg^{2+} sensor (B) before and after regeneration at low or high pH. The fold of fluorescence enhancement after adding 2 mM adenosine (C) or 2 μM Hg^{2+} (D). Noted that black arrows shown in kinetic plots indicated the time points where target molecules were added.

Ideally, all targets bounded aptamers in the supernatant should be washed away with pH 7.5 buffer once the signal reached plateau. However, the sample washed with pH 7.5 buffer also showed a small increase after regeneration. The only plausible explanation is that not all the aptamers were desorbed from GO in the presence of 2 mM adenosine. To verify this, 4 μM of the cDNA of the aptamer was used to desorb the FAM-labeled aptamer DNA (black dash line). For adenosine sensor, the K_d for the cDNA binding should be smaller than 10^{-18} M[161], which is 12 orders of magnitude higher than that for adenosine binding. As shown in Figure 3.3A (black curve), the aptamer desorbed by adenosine was only about half of that desorbed by the cDNA (black dash curve). Similarly, desorption induced by 2 μM Hg^{2+} was also incomplete and was only ~40% of that by adding the cDNA (Figure 3.3B, black dash curve) This experiment confirmed the fluorescence signal observed after regeneration at pH 7.5 was attributed to these residual aptamers left on the GO surface.

The fact that the pH 3.5 samples showed a much higher fluorescence after regeneration supported that a low pH was crucial for the reverse binding process. However, it was noted that the regeneration was incomplete even for the pH 3.5 samples. If the fold of fluorescence enhancement was compared, the change for the regenerated sensor was comparable to that for the freshly prepared one (Figure 3.3C & D, black bars). On the other hand, a significant drop was observed for the samples regenerated in the pH 7.5 buffer (gray bars). The incomplete fluorescence recovery was probably due to the lost of GO during the centrifugation/washing steps. More importantly, the result also indicated that the performance of the aptamer/GO sensor was not affected by regeneration.

3.2.4 Logic Gate

Four aptamer/GO samples were prepared to be at high (7.5) or low (3.5) pH in the presence of high (2 mM) or low (0 mM) adenosine. After centrifugation, the supernatant fluorescence was then measured at pH 8.5 to avoid the false negative results. We found that high fluorescence was achieved only at high pH and high adenosine (Figure 3.4A). This system therefore acts as an **AND** gate (Figure 3.4B). This study also showed that the pH effect predominate at low pH; no desorption occurred even in the presence of adenosine.

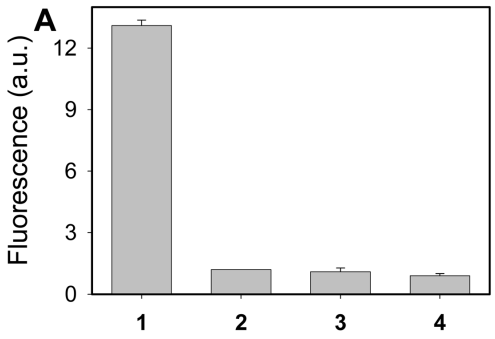

B

Sample ID	pH	Adenosine	Fluorescence
1	High	High	High
2	High	Low	Low
3	Low	High	Low
4	Low	Low	Low

Figure 3.4 Logic gate based on adenosine DNA aptamers. (A) The supernatant fluorescence intensity of adenosine aptamer/GO complex in different pH and adenosine conditions. (B) Tabulated results in (A), where high pH = 7.5, low pH = 3.5, high adenosine = 2 mM and low adenosine = 0.

3.2.5 ssDNA/dsDNA Separation without Gel Electrophoresis

To demonstrate the concept, the supernatants of the samples were loaded on a 15% non-denaturing polyacrylamide gel to see the efficiency of separation. Different ratio of ssDNA and dsDNA mixtures were incubate with GO for short period of time (~ 20 min). As shown in Figure 3.5, ssDNA and dsDNA fluorescence bands were observed at different distance on the gel (left side of the image) based on their molecular weight. When the

mixtures was incubated with GO, all the ssDNA adsorbed on the surface. Thus, only the dsDNA fluorescence bands were observed (right side of the image). The result suggested that ssDNA/dsDNA can be quickly and easily separated by this method.

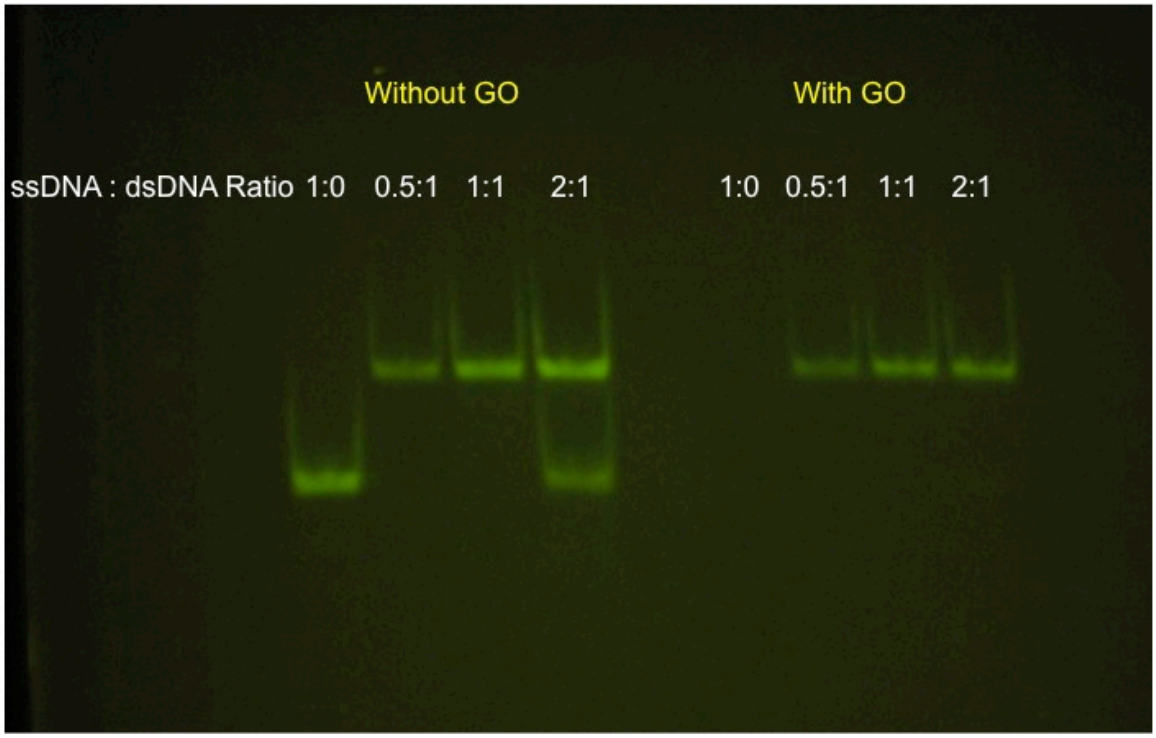

Figure 3. 5 Gel electrophoresis image of ssDNA/dsDNA mixtures at different ratio with or without GO incubation.

3.3 Conclusion

With the information obtained from the DNA/GO interaction studies, we knew that a precise control of binding at the bio-nano interface can be achieved. Herne, we demonstrated the synergistic pH effect on the binding of aptamer to its target and to GO. In this system, it is possible to achieve sensor regeneration without covalent immobilization. This method should work for small molecule and metal ion targets. However, DNA or protein targets may also bind to the GO surface with a high affinity. Thus, effective

removal of such target molecules may not be achieved. The same synergistic pH effect was also applied to logic gate system. In another example, we also demonstrate the intrinsic selectivity of the GO can be utilized for ssDNA/dsDNA separation kit. Without the need for gel electrophoresis, dsDNA can be easily separated under 20 min.

3.4 Experimental Section

3.4.1 Chemicals

All DNA samples were purchased from Integrated DNA Technologies (Coralville, IA). For sensor regeneration experiment, the adenosine and Hg^{2+} were used. Adenosine aptamer sequence is FAM-ACC TGG GGG AGT ATT GCG GAG GAA GGT; Hg^{2+} aptamer sequence is FAM-TTC TTT CTT CCC CTT GTT TGT T. The DNAs used in gel electrophoresis have the following sequence: 24-mer, FAM-ACG CAT CTG TGA AGA GAA CCT GGG; 24-mer cDNA, TGC GTA GAC ACT TCT CTT. For ITC analysis, non-modified adenosine aptamer (ACC TGG GGG AGT ATT GCG GAG GAA GGT) was used. All the sequences are listed from the 5′ to 3′-end. Sodium chloride, magnesium chloride, sodium acetate, 4-Morpholineethanesulfonate (MES), 4-(2-hydroxyethyl)piperazine-1-ethanesulfonate (HEPES), and Tris(hydroxymethyl)aminomethane (Tris) were purchased from Mandel Scientific (Guelph, Ontario, Canada). Sulfuric acid, potassium persulfate, phosphorous pentoxide, hydrogen peroxide, potassium permanganate were purchased from Sigma-Aldrich. Acetic acid and hydrochloric acid were purchased from VWR. Graphite flakes were purchased from Fisher. Millipore water was used for all the experiments. GO was prepared as

described previously and was provided by Dr. Maheshwari.

3.4.2 ITC Analysis on Adenosine Aptamer/Adenosine Binding

For the titration measurement, 250 μL of 60 μM adenosine aptamer was load into the cell chamber and 40 μL of 1.5mM adenosine is needed in the syringe. The experiments were conducted at 25 °C. 150 mM NaCl with 25 mM sodium citrate buffer (pH 3.5 & 5.5) or 25 mM HEPES (pH 7.5) were used to study the pH effect on adenosine aptamer/adenosine binding efficiency. To obtain binding curve at pH 3.5, 10 mM adenosine was needed. Noted that adenosine aptamer was pre-heated at 95°C for ~ 1 minute and gradually cooled to room temperature then storing in ice bath before the analysis. The amount of released heat was measurement after each addition by using MicroCal 200.

3.4.3 Salt and pH-dependent Study on the Adenosine Aptamer/GO Binding

In this experiment, adenosine aptamer was used. 500 nM of adenosine aptamer was incubated with 100 μg/ml of GO in 150mM NaCl with 25 mM buffer at various pH (pH 3.5 ~ 7.5). To study the effect of the ionic strength, aptamer and GO were also incubated in 25mM buffer at various pH. After 1-hour incubation, the samples were centrifuged at ~15000 RPM for 20min and the supernatants were collected. The supernatants were then diluted 5 times with HEPES buffer for fluorescence measurement using micro-plate reader (Tecan Infinite F200 Pro). The fluorescence values were compared with the 100nM aptamer for calculating adsorption efficiency.

3.4.4 Potential Applications

3.4.4.1 Aptamer-GO Sensor Regeneration

The biosensor was prepared by incubating 500nM of adenosine aptamer with 100 μg/ml of GO in 150 mM NaCl/25 mM HEPES/1 mM $MgCl_2$ buffer. The mixture was washed once with the same buffer to ensure any unbound aptamers was removed. The biosensor was then re-dispersed with the same buffer. 2 μM of target was added into 20 μg/ml of Aptamer-GO sensor and the fluorescence was recorded. To regenerate the biosensor, 500 mM of sodium citrate (pH 3.5) was used to acidify the samples. The samples were incubated in this low pH buffer for ~ 40 min. The samples then were centrifuged and the supernatants were discarded. The biosensor was washed with 500mM HEPES once before re-dispersed in 150 mM NaCl/25 mM HEPES/1 mM $MgCl_2$ buffer for fluorescence measurement.

3.4.4.2 Logic gate

In this experiment, adenosine aptamer was used. Four aptamer/GO samples were prepared in either pH 3.5 or pH 7.5 buffers. In addition, 2 mM adenosine was added to two of the samples. After centrifugation, the supernatant fluorescence was then measured at pH 8.5 to avoid pH-related FAM fluorescence issue.

3.4.4.3 ssDNA/dsDNA Separation kit

ssDNA/dsDNA mixtures with different ratio were prepared. The mixtures were

then incubated with 100 μg/ml GO for ~ 20 min. Samples were then centrifuged at 14000 RPM and supernatants were collected and loaded into 15% non-denaturing polyacrylamide gel. Gel electrophoresis was running at 500 V for an hour. The gel was illuminated with Invitrogen Safe Imager 2.0 Blue-Light Transilluminator and the image was taken with digital camera.

Chapter 4. Distance Dependent Fluorescence Quenching of Graphene Oxide

4.1 Introduction

Like CNTs,[138, 162, 163] GO is an excellent quencher for adsorbed fluorophores.[101] In addition, it demonstrated high quenching efficiency for various fluorophores ranging from green, red, and far red emitting dyes to quantum dots.[101, 103, 104] In the presence of its cDNA, the fluorescence was recovered due to duplex formation and desorption.[104] At the same time, the fluorophore-to-GO distance increased from zero to infinite to give the maximal fluorescence enhancement. Based on these understandings, many optical sensors have been designed were using the similar mechanism for the detection. Although the optical applications were greatly emphasized, little is known about the distance-dependent fluorescence quenching within a few nanometers above the GO surface. In fact, many of these reports were based on theoretic calculation.[164, 165] Such information is important for the rational design of covalently linked probes.

Compared to sensors that were based on simple physisorption of probes, there are several advantages of using covalent linked probes. First of all, such sensors are reversible and can be used for continuous monitoring for a long time and even under flow conditions. Secondly, covalent sensors are less prone to non-specific displacement that causes false positive results. Last but not least, these types of sensors can be easily regenerated with simple washing steps.

Studying distance-dependent fluorescence property is also crucial for

understanding the fundamental quenching mechanism. Based on theoretical calculations, Sebastian K. and Swathi R. predicted that quenching by graphene followed a d-4 dependency, where d was the distance between the dye and the GO.[164-166] This is similar to the so-called nanosurface energy transfer (NSET) studied using gold nanoparticles.[167-170] To date, no experimental work on GO was carried out.

Once DNA formed a rigid structure, it can often achieve a precise distance control at nanometer scale. To have a systematic understanding of these important questions about the quenching mechanism, eight amino and 6-carboxyfluorescein (FAM) dual labeled DNA probes with varying DNA lengths and fluorophore positions was employed. These probes were covalently attached to the GO surface and their respective cDNA was added to form rigid duplexes (Scheme 4.1A). Given the complexity of the system brought by the planar nature of GO and its surface heterogeneity, four different aspects: steady-state fluorescence spectroscopy, fluorescence lifetime spectroscopy, fluorescence microscopy and fluorescence lifetime imaging were studied. This represents the first work of using DNA to systematically study the distance-dependent fluorescence quenching on GO.

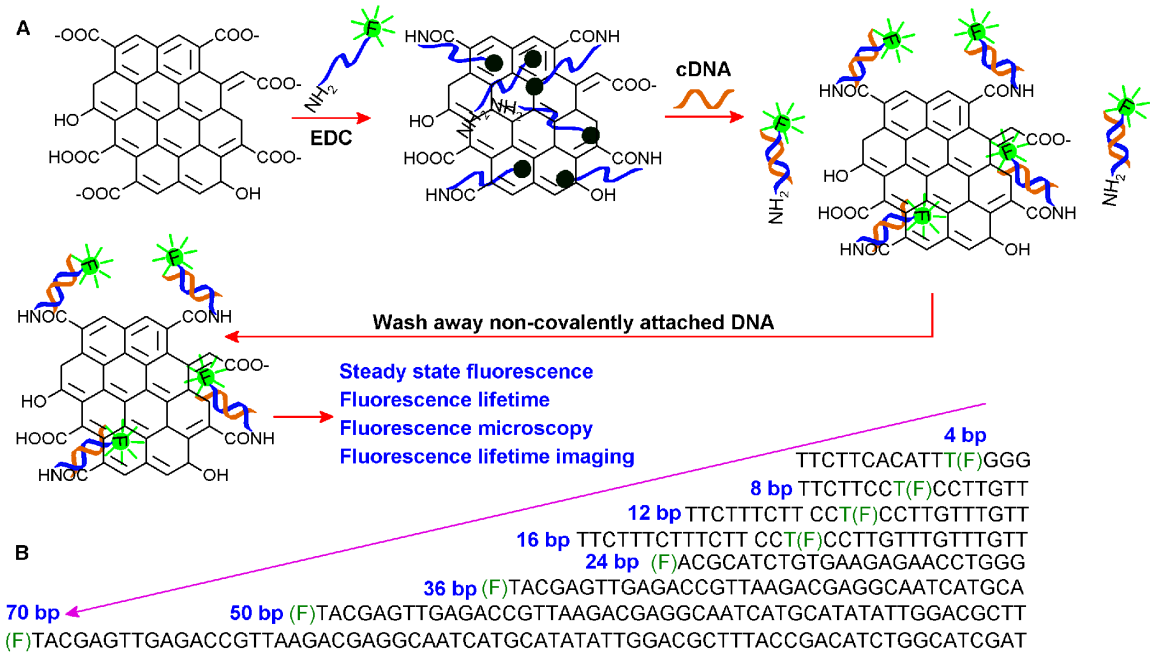

Scheme 4.1 (A) Schematic illustration of distance-dependent fluorescence quenching study. (B) Sequence and fluorophore position of all eight ssDNA.

4.2 Results and Discussion

4.2.1 Steady-State Fluorescence Spectra

All eight ssDNAs were modified with amino group on the 3′-end and FAM either in the middle or at the 5′- end. The details of DNA sequences and modifications can be seen in Scheme 4.1B. These DNAs in the system were designed such that the FAM and GO were separated by 4 to 70 base pairs (bp) after forming the duplex DNAs. Each of the dual labeled ssDNAs was reacted with GO in the presence of EDC to form covalent amide linkages. To maximize the covalent bonding efficiency, excess of DNAs were added into the reaction. Once the reaction was complete, the non-associated DNAs were first removed

using centrifugation. Because of the surface heterogeneity, the DNAs associated with GO can be divided into two populations: chemisorbed through forming the amide bond and physisorbed through hydrophobic interactions.

For sensing applications, steady-state fluorescence spectroscopy is one of the most often used techniques and it provides information about fluorescence quantum yield and spectrum shape. The steady-state fluorescence spectra of these samples are shown in Figure 4.1A. Samples were excited at 485 nm and the emission spectra from 500 to 600 nm were collected. The emission intensity at 520 nm was plotted as a function of the FAM position. Without any cDNA presence, the background fluorescence was close to zero for all eight samples (Figure 4.1B, blue dots). The low fluorescence indicated that the DNAs were tightly adsorbed by the GO surface to result in a strong quenching.

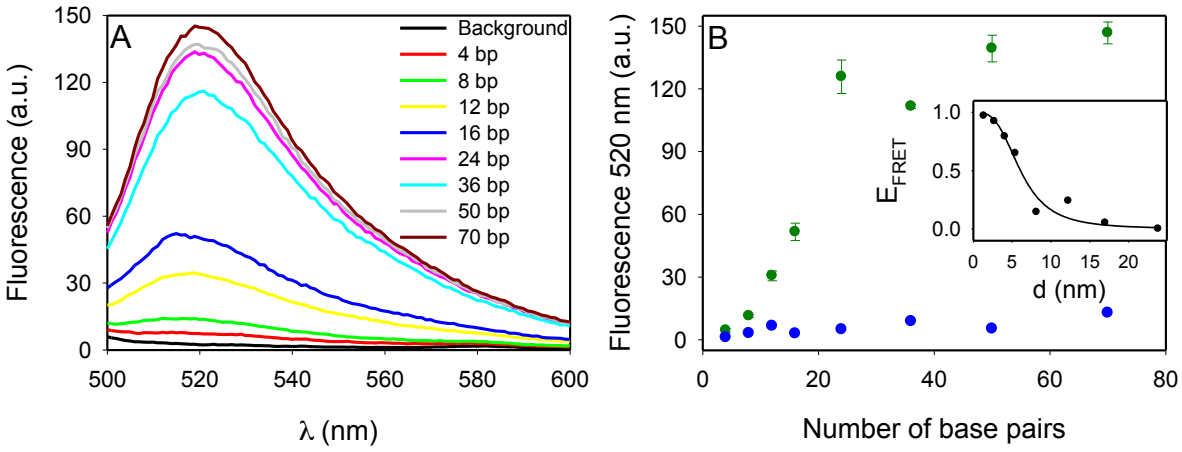

Figure 4.1 (A) Steady-state fluorescence spectra of the covalently linked FAM-modified DNAs after forming duplex with the cDNAs in 100mM NaCl & 25mM HEPES (pH 7.6). (B) The 520 nm peak intensity as a function of the FAM position in terms of the number of base pairs before (blue dots) and after (green dots) adding the cDNAs. Inset: quenching efficiency as a function of calculated FAM-to-GO distance (assuming DNA vertical orientation) and its best fitting into an energy transfer model. E_{FRET} equals to the quenching efficiency.

Since we were only interested in the fluorescence of covalently linked DNAs in this study, any non-covalently linked DNAs should be removed to prevent any false signal. As mentioned in previous chapter, these physisorbed DNAs were very difficult to remove just by simple washing. The most efficient way to separate these unwanted DNAs from the system is to use cDNA. Once the cDNAs were added, it formed duplex with these ssDNAs on the GO surface. For covalently linked ssDNAs, the duplex will still attach to the surface with their conformation being a rigid rod. However, the physically adsorbed DNA will desorb from the surface after forming duplex. These duplex in the solution can then be easily removed through centrifugation. To ensure that the non-covalently adsorbed DNAs were completely removed from the system, more cDNAs were added and this process was repeated three times. At the end of this process, only ds-DNAs immobilized on GO were expected to be present.

With the final addition of the cDNAs, samples were measured again with fluorometer. Increased fluorescence over background was observed for all the samples (Figure 4.1B, green dots). As the FAM-to-GO distance increases, the fluorescence intensity also increases. The result suggested that the GO surface acted as an energy acceptor to quench FAM in a distance-dependent manner. The increase intensity ranged from ~ 4-fold for the 4-12 bp samples to > 10-fold for the 16-70 bp ones were observed. In addition, this experiment indicated that effective sensors can still be obtained even with covalently linked probes. As seen in Figure 4.1A, even 4 bp can be detected due to the extremely low background fluorescence of DNA/GO complex. However, the final FAM-to-GO distance after the reaction should be greater than 12 bps to achieve a good S/N.

According to the literature, the persistence length of a β-form ds-DNA is ~50

nm.[171] With the longest DNA in this work is 70 bp (= 23.8 nm), the duplex can still be considered to be a rigid rod. If all the duplexes had oriented vertically with respect to the GO surface, the data presented here would provide some information on the distance-dependent quenching. Noted that once the number of bp is greater than 50, the fluorescence enhancement is limited. With the assumption that the quenching efficiency (Q) is zero for the 70 bp sample, the quenching efficiency (the same as FRET efficiency) of the rest can be calculated based on equation 4.1 where F_D and F_{DA} are the fluorescence intensity of the DNA in the absence and presence of GO respectively.

$$E_{FRET} = 1 - \frac{F_{DA}}{F_D} \tag{4.1}$$

As shown in the inset of Figure 4.1B, the best fit to the equation 4.2[164, 165] where resulted in n = 3.3 and d_0 = 6.1 nm, where d is the FAM-to-GO distance and d_0 is the Förster distance where Q = 0.5.

$$Q = \frac{1}{[1+(d/d_0)^n]} \tag{4.2}$$

In the previous theoretical study, Swathi and Sebastian determined that dye to graphene has (distance)$^{-4}$ dependence.[164, 165] With this constrain, we obtained d_0 = 6.0 nm. While the experimental n value is close to the theoretical value published, it needs to be addressed that the value above does not represent an accurate model since the entire calculation was based on the assumption that the quenching efficiency for the 70-mer duplex was zero. More importantly, the FAM-to-GO distance was estimated simply based on the number of base pairs. As will be discussed later, neither of these assumptions was true. In the case of tilted dsDNA after binding, the angle between the DNA and GO was no

longer perpendicular. As a result, the distance derived from the DNA length was longer than the actual FAM-to-GO distance. In addition, the steady-state fluorescence intensity relied heavily on the EDC coupling efficiency and final GO concentration. With all the centrifugation and washing steps, the GO concentration was expected to be slightly different across the samples. Even though the intensity measurement cannot provide great details about the quenching, the plot clearly indicated that quenching was distance-dependent.

4.2.2 Fluorescence Microscopy Analysis

An important application of the DNA/GO conjugate is for cellular and biomedical imaging.[116, 121, 125, 172] For example, DNA and aptamer-based probes can be used to measure gene and protein expression as well as metabolite concentration. With covalent linkage, reversible and long-term monitoring of local analytes concentration change becomes feasible. To demonstrate the concept, these samples were observed under a fluorescence microscope. By analyzing the individual GO sheets, the effect of sample concentration difference that might present in a cuvette-base measurement can be eliminated. As shown in Figure 4.2A-H, the increasing fluorescence intensity is correlated with increasing DNA length. The transition observed here is also consistent with the fluorescence spectroscopy results. Under optimized condition, a distance of ~8-12 bp was the minimum requirement to generate a readable signal. To increase the S/N of the images, longer DNAs are preferred. The fluorescence intensity was quantified in Figure 4.2I. As expected, no background fluorescence was observed in the absence of cDNA. This experiment confirmed that a strong signal for imaging could be generated even if the DNA

probe did not completely desorb from the surface. As long as the fluorophore is several base pairs (e.g. from 8 to 16) above the GO, a significant signal change can be easily detected.

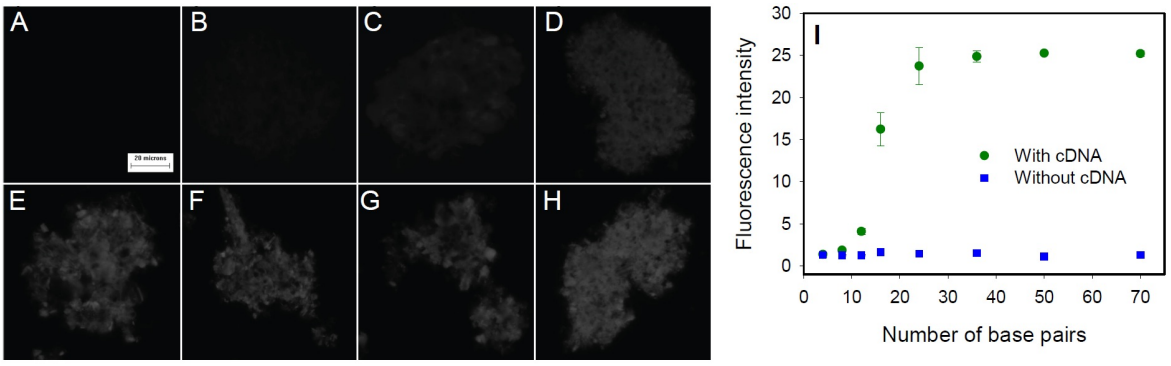

Figure 4.2 Fluorescence micrographs (40x objective) for eight GO samples. Microscopic images of (A) 4 bp, (B) 8 bp, (C) 12 bp, (D) 16 bp, (E) 24 bp, (F) 36 bp, (G) 50 bp, & (H) 70 bp. The scale bar shown in (A) is 20 µm and is shared by all the figures. (I) Fluorescence intensity quantification before and after cDNA addition.

4.2.3 Fluorescence Lifetime Decay

To exam the quenching efficiency more closely, fluorescence lifetime spectroscopy was used to study these FAM-labeled DNA-functionalized GOs. After incubating with cDNAs, the lifetime decay traces were collected. As shown in Figure 4.3A, a FAM-labeled DNA freely dispersed in solution had a single exponential decay with a lifetime of 4.05 ns (green line) and all the DNA/GO conjugates displayed faster decay than the free FAM-labeled DNA. The result clearly indicated the quenching mechanism of FAM/GO is dynamic. Interesting, the data also showed that none of the GO samples followed single exponential lifetime decay. This observation suggested the presence of different populations in terms of the fluorophore environment. The best fit was obtained using a

double exponential decay model for all the samples. For the 4 to 24 bp samples, the long lifetime component was minor in population (5-20%) and these lifetime values were close to that of the free FAM. It indicated the small population was not significantly affected by dynamic quenching. On the other hand, the shorter lifetime component had lifetime gradually increased from ~0.3 ns for 4 bp to ~1 ns for 24 bp. For longer DNAs (> 24 bps), the analysis became more complicated. The population of the short and long lifetime components were more comparable. In addition, the short lifetime component stopped increasing when it reached a value of ~1.3 ns.

FRET or quenching efficiency can also be calculated using the fluorescence lifetime data based on equation 4.3, where τ and τ_0 are the fluorescence lifetime in the presence and absence of quencher, respectively.[173]

$$Q = 1 - \frac{\tau}{\tau_0} \tag{4.3}$$

In the absence of GO, τ_0 was determined to be 4.05 ns for FAM-labeled free DNA. As shown in Figure 4.3B, the quenching efficiency decreased with increasing DNA length but it stopped at ~0.7 when the DNA bp number reached 36 (~12.2 nm). While the length of the DNA almost doubled from 36-mer to 70-mer, the short lifetime component barely changed.

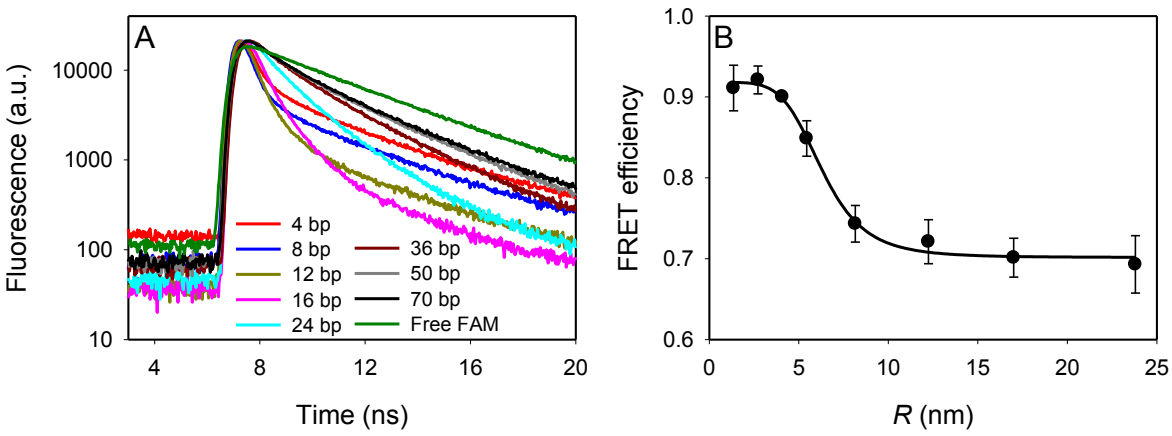

Figure 4.3 Fluorescence lifetime spectra. (A) Decay traces of covalently linked FAM DNAs with cDNAs added. (B) Quenching efficiency plotted as a function of the FAM-to-amino distance based on the assumption of vertical DNA orientation.

As mentioned earlier in the chapter, the FAM-labeled DNAs were assumed to be in vertical orientation. However, the data suggested the possible scenario that DNAs did not stand up vertically with respect to the GO surface as we expected. It is likely that the longer the DNA, the smaller the angle between the DNA and the GO surface. Thus, the actual FAM-to-GO distance is much shorter than we estimated initially. Moreover, it also confirmed that there are some weak binding affinity between the dsDNAs and the GO. Unfortunately, the non-vertical DNA orientation made it impossible to obtain an accurate Förster distance (d_0) between FAM and GO. As a result, the curve in Figure 4.3B can only serves as a working model, similar to the one shown in Figure 4.1B.

4.2.4 Fluorescence lifetime imaging

The above fluorescence lifetime experiment clearly indicated the existence of

different DNA populations on the GO surface. It is very important to further exam the spatial distribution of fluorescence lifetime so that the physical origin of these different populations may be assigned. Fluorescence lifetime imaging technique was employed and only the 16 and 70 bp samples were studied. With this technique, the FAM fluorophore was excited using multi-photon excitation to achieve a high spatial resolution. The sample images are presented in Figure 4.4. Orange color represented short lifetime components and blue represented long lifetime components. Initial observation confirmed that the lifetime distribution was inhomogeneous on the surface as previous suggested. The lifetime distribution in the black box of Figure 4.4A was shown in Figure 4.4B. Although the overall lifetime was ~0.5 ns, the 16 bp sample appeared to have few long lifetime spots. The value is consistent with the lifetime spectroscopy data in Figure 4.3. More importantly, the image could explain that the long lifetime component observed in the spectrometer was due to these long lifetime spots instead of free DNAs in solution. Like the 16 bp sample, the distribution was highly heterogeneous for 70 bp sample (Figure 4.4C). Unsurprisingly, the overall lifetime increased with a longer distance. The lifetime distribution (Figure 4.4D) showed that most area had a lifetime close to 1 ns.

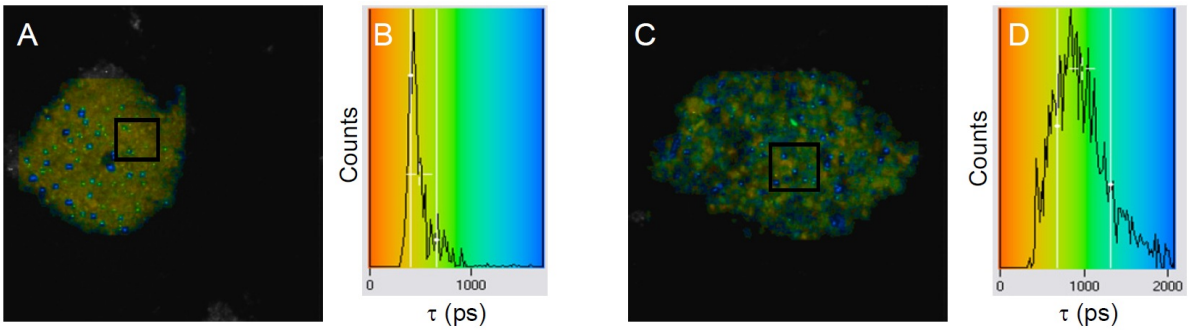

Figure 4.4 Fluorescence lifetime images. Fluorescence lifetime distribution and histogram of the 16-mer (A & B) and 70-mer (C & D) samples.

It is known that pristine graphene surface is homogeneous but extremely hydrophobic. To disperse in water, GO with surface oxygen species were prepared. However, oxidation makes GO surface heterogeneous.[142, 144, 174-177] It is well known that graphene is better quencher than GO. For the DNAs attached to the highly oxidized regions, the quenching efficiency was low and the DNA tended to stay away from the surface due to electrostatic repulsion between surface carboxylate and DNA backbone. Thus, these regions appeared to have longer lifetime. On the other hand, DNAs linked to the carbon rich regions where the local surface around the DNA was less charged. Consequently, DNA might be closer to the surface. The quenching efficiency of these carbon rich regions is known to be very high, resulting in strong dynamic quenching even for the 70-mer DNA.[164, 165] Since we are interested in quenching caused by graphene instead of the highly oxidized regions, only the short lifetime component was plotted in Figure 4.3B.

4.4 Conclusion

Initially, our goal was to use the advantage of covalently linkage to evaluate the fluorescence quenching between FAM-DNA and GO. With the assumption that DNA duplexes are in vertical orientation on the GO surface, Förster distance could be determined. However, the results here indicated that our initial assumption was not correct. More importantly, fluorescence lifetime does not appear to be an attractive analytical method in the covalent DNA/GO system. Resolving multi-exponential lifetime decay is known to be challenging and it is prone to errors. Since this system is extremely

heterogeneous, it is difficult to obtain accurate values. For instance, heterogeneous surface gave different quenching efficiencies. Also, the angle between DNA and GO after duplex formation can vary. This adverse effect can especially be seen in longer DNA length. The nature of this interaction is likely to be a combination of van de Waals attraction and electrostatic repulsion. Given these considerations, the interpretation of lifetime change is difficult and is unlikely to be analytically useful.

The understanding about the DNA and GO interaction can be summarized in Figure 4.5. Amino-modified ssDNAs were immobilized around the highly oxidized regions or in the carbon rich regions. The attached fluorophores were completely quenched due to the hydrophobic and π-π stacking interaction between DNA and GO. Addition of the cDNAs resulted in dsDNAs formation and partially left the GO surface. The angle between the dsDNAs and GO was less than 90°, especially for those on the carbon-rich regions. The longer the DNA, the smaller the angle (e.g. θ1 < θ2 < 90° in Scheme 4.2) will be.

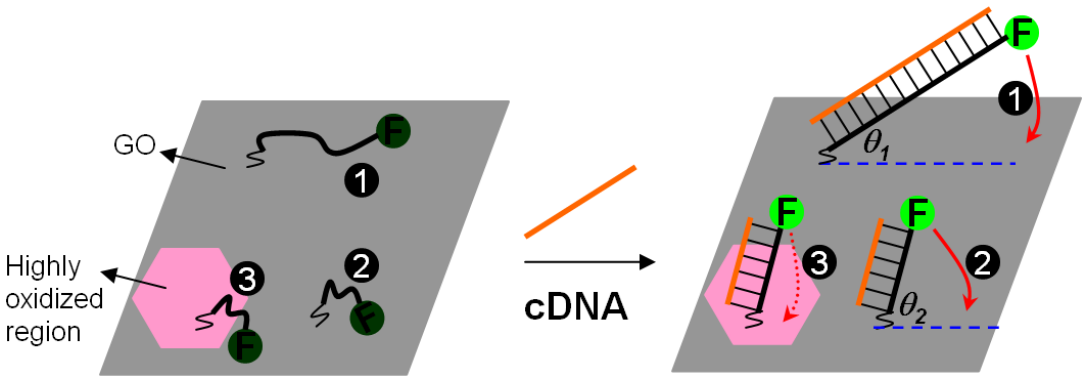

Scheme 4. 2 Schematics of covalently immobilized DNA probes and the formation of dsDNA on GO. DNA 1 is longer than DNA 2. DNA 3 is close to the highly oxidize region. It is likely that $\theta_1 < \theta_2 < 90°$.

Finally, it has been previously predicated through theoretical calculation that the quenching efficiency of graphene follows d^{-4}.[164, 165] The same distance-dependent quenching by gold nanoparticles was also reported.[167, 168] However, the mechanism of quenching by the metal and by the π system is fundamentally different. The dynamic quenching nature by CNTs surface has also been studied using covalently linked pyrenes, but the exact mechanism is still under investigation.[178-180] With the planar nature of GO and the flexible linker for attaching DNA to GO, it is impossible to obtain a precise FAM-to-GO distance based simply on the DNA length. The only conclusion that can be drawn here is that quenching between FAM-DNA and GO is distance-dependent. It is known that DNA/GO complex showed extremely low background fluorescence in the absence of cDNA. Even though FRET between the fluorophore and GO result in reduced fluorescence intensity, a high signal-to-background ratio can still be obtained even with the presence of significant quenching. To achieve a precise distance, more rigid DNA structures are needed.[181, 182]

4.4 Experimental Section

4.4.1 Chemicals

All DNA samples were purchased from Integrated DNA Technologies (Coralville, IA). The DNA sequences and modifications are listed in Figure 3.1B. All the DNAs were purified by HPLC except for the 24 and 36-mers. Sodium chloride, magnesium chloride, 4-Morpholineethanesulfonate (MES), 4-(2-hydroxyethyl)piperazine-1-ethanesulfonate (HEPES), were purchased from Mandel Scientific (Guelph, Ontario, Canada). *N*-(3-

Dimethylaminopropyl)-*N*′-ethylcarbodiimide hydrochloride (EDC·HCl) was purchased from Sigma-Aldrich. Millipore water was used for all the experiments. GO was prepared as described previously and was provided by Dr. Maheshwari.

4.4.2 Covalent attaching DNA to GO

The one-step conjugation was carried out in a glass vial with a final volume of 500 μL containing 100 μg/mL GO, 2 μM amino-modified DNA, 10mM EDC·HCl (freshly prepared), 25mM NaCl and 25 mM MES, pH 6.0. The reaction was carried out for 3 hr at room temperature in the dark with continuous magnetic stirring. Any excess of unreacted ssDNA in the supernatant were removed by centrifugation at 15000 rpm for 20 min. The DNA/GO conjugates were then washed in 500 μL of water twice to further remove non-covalently adsorbed DNA. Finally, the conjugates were dispersed in 100mM NaCl with 25 mM HEPES (pH 7.6). Final GO concentration was maintained at 100 μg/mL and stored at 4 °C before use.

4.4.3 Steady-state fluorescence spectra

Steady state fluorescence spectra were collected using a Varian Eclipse spectrofluorometer. The excitation wavelength was set at 485 nm and the emission from 500 to 600 nm was collected. The GO concentration in the cuvette was 20 μg/mL and had been repeated treated with 4 μM cDNA for three times to completely desorb non-covalently attached DNAs. All the reactions were carried out in buffer A. After reacting

with cDNA, the samples were centrifuged at 15000 rpm for 20 min and the supernatant was carefully removed.

4.4.4 Fluorescence lifetime spectroscopy

400μl of 20 μg/mL GO sample was used for lifetime measurement. Fluorescence lifetime was collected using PicoQuant FluoTime 100 spectrofluorometer. The laser light source was set at 460-480nm for the excitation. 520nm band pass filter was chosen for data collection. The data were fit to a double exponential decay.

4.4.5 Fluorescence microscopy

The GO samples were observed using Leica DMI 3000B inverted microscope with Hamamatsu ORCA-R^2 camera system. The GO samples were concentrated to ~200 μg/mL and 2 μL of these samples were spotted on a glass slide. The samples were imaged after putting on a cover slip. The cube for green fluorescence imaging was used. The fluorescence microscopic pictures were taken under the 40× objective with an exposure time of 10 sec.

4.4.6 Fluorescence lifetime imaging

The fluorescence lifetime images were captured using Leica DM 6000B microscope with Leica TCS SP5 system using the 63× (glycerol) objective. The excitation

source was a multiphoton IR laser.

References

(1) Fernie, A. R.; Trethewey, R. N.; Krotzky, A. J.; Willmitzer, L. Innovation - Metabolite profiling: from diagnostics to systems biology. *Nature Reviews Molecular Cell Biology* **2004**, *5*, 763-769.

(2) Sreekumar, A.; Poisson, L. M.; Rajendiran, T. M.; Khan, A. P.; Cao, Q.; Yu, J. D.; Laxman, B.; Mehra, R.; Lonigro, R. J.; Li, Y.; Nyati, M. K.; Ahsan, A.; Kalyana-Sundaram, S.; Han, B.; Cao, X. H.; Byun, J.; Omenn, G. S.; Ghosh, D.; Pennathur, S.; Alexander, D. C.; Berger, A.; Shuster, J. R.; Wei, J. T.; Varambally, S.; Beecher, C.; Chinnaiyan, A. M. Metabolomic profiles delineate potential role for sarcosine in prostate cancer progression. *Nature* **2009**, *457*, 910-914.

(3) Gowda, G. A. N.; Zhang, S. C.; Gu, H. W.; Asiago, V.; Shanaiah, N.; Raftery, D. Metabolomics-based methods for early disease diagnostics. *Expert Review of Molecular Diagnostics* **2008**, *8*, 617-633.

(4) Mertz, W. The Essential Trace-Elements. *Science* **1981**, *213*, 1332-1338.

(5) Jarup, L. Hazards of heavy metal contamination. *Br. Med. Bull.* **2003**, *68*, 167-182.

(6) Dettmer, K.; Aronov, P. A.; Hammock, B. D. Mass spectrometry-based metabolomics. *Mass Spectrom. Rev.* **2007**, *26*, 51-78.

(7) Soininen, P.; Kangas, A. J.; Wurtz, P.; Tukiainen, T.; Tynkkynen, T.; Laatikainen, R.; Jarvelin, M.; Kahonen, M.; Lehtimaki, T.; Viikari, J.; Raitakari, O. T.; Savolainen, M. J.; Ala-Korpela, M. High-throughput serum NMR metabonomics for cost-effective holistic studies on systemic metabolism. *Analyst* **2009**, *134*, 1781-5.

(8) Anderson, N. L.; Anderson, N. G. The human plasma proteome - History, character, and diagnostic prospects. *Molecular & Cellular Proteomics* **2002**, *1*, 845-867.

(9) Lenz, E. M.; Wilson, I. D. Analytical strategies in metabonomics. *Journal of Proteome Research* **2007**, *6*, 443-458.

(10) Prange, A.; Jantzen, E. Determination of Organometallic Species by Gas-Chromatography Inductively-Coupled Plasma-Mass Spectrometry. *J. Anal. At. Spectrom.* **1995**, *10*, 105-109.

(11) Cai, Y.; Bayona, J. M. Determination of Methylmercury in Fish and River Water Samples using In-Situ Sodium Tetraethylborate Derivatization Following by Solid-Phase Microextraction and Gas-Chromatography Mass-Spectrometry. *Journal of Chromatography a* **1995**, *696*, 113-122.

(12) Jimenez, M. S.; Sturgeon, R. E. Speciation of methyl- and inorganic mercury in biological tissues using ethylation and gas chromatography with furnace atomization plasma emission spectrometric detection. *J. Anal. At. Spectrom.* **1997**, *12*, 597-601.

(13) Gerbersmann, C.; Heisterkamp, M.; Adams, F. C.; Broekaert, J. A. C. Two methods for the speciation analysis of mercury in fish involving microwave-assisted digestion and gas chromatography atomic emission spectrometry. *Anal. Chim. Acta* **1997**, *350*, 273-285.

(14) Achterberg, E. P.; Braungardt, C. Stripping voltammetry for the determination of trace metal speciation and in-situ measurements of trace metal distributions in marine waters. *Anal. Chim. Acta* **1999**, *400*, 381-397.

(15) Jelen, F.; Yosypchuk, B.; Kourilova, A.; Novotny, L.; Palecek, E. Label-free determination of picogram quantities of DNA by stripping voltammetry with solid copper amalgam or mercury electrodes in the presence of copper. *Anal. Chem.* **2002**, *74*, 4788-4793.

(16) Yantasee, W.; Lin, Y. H.; Zemanian, T. S.; Fryxell, G. E. Voltammetric detection of lead(II) and mercury(II) using a carbon paste electrode modified with thiol self-assembled monolayer on mesoporous silica (SAMMS). *Analyst* **2003**, *128*, 467-472.

(17) Bloom, N.; Fitzgerald, W. F. Determination of Volatile Mercury Species at the Picogram Level by Low-Temperature Gas-Chromatography with Cold-Vapor Atomic Fluorescence Detection. *Anal. Chim. Acta* **1988**, *208*, 151-161.

(18) Harrington, C. F. The speciation of mercury and organomercury compounds by using high-performance liquid chromatography. *Trac-Trends in Analytical Chemistry* **2000**, *19*, 167-179.

(19) Kroger, S.; Piletsky, S.; Turner, A. P. F. Biosensors for marine pollution research, monitoring and control. *Mar. Pollut. Bull.* **2002**, *45*, 24-34.

(20) Popovtzer, R.; Neufeld, T.; Biran, N.; Ron, E. Z.; Rishpon, J.; Shacham-Diamand, Y. Novel integrated electrochemical nano-biochip for toxicity detection in water. *Nano Letters* **2005**, *5*, 1023-1027.

(21) Chaerkady, R.; Pandey, A. Applications of proteomics to lab diagnosis. *Annual Review of Pathology-Mechanisms of Disease* **2008**, *3*, 485-498.

(22) Ivnitski, D.; Abdel-Hamid, I.; Atanasov, P.; Wilkins, E. Biosensors for detection of pathogenic bacteria. *Biosens. Bioelectron.* **1999**, *14*, 599-624.

(23) Iqbal, S. S.; Mayo, M. W.; Bruno, J. G.; Bronk, B. V.; Batt, C. A.; Chambers, J. P. A review of molecular recognition technologies for detection of biological threat agents. *Biosens. Bioelectron.* **2000**, *15*, 549-578.

(24) D'Orazio, P. Biosensors in clinical chemistry. *Clinica Chimica Acta* **2003**, *334*, 41-69.

(25) Heller, A.; Feldman, B. Electrochemical glucose sensors and their applications in diabetes management. *Chem. Rev.* **2008**, *108*, 2482-2505.

(26) Jelinek, R.; Kolusheva, S. Carbohydrate biosensors. *Chem. Rev.* **2004**, *104*, 5987-6015.

(27) Jung, Y.; Jeong, J. Y.; Chung, B. H. Recent advances in immobilization methods of antibodies on solid supports. *Analyst* **2008**, *133*, 697-701.

(28) Tuerk, C.; Gold, L. Systematic Evolution of Ligands by Exponential Enrichment - Rna Ligands to Bacteriophage-T4 Dna-Polymerase. *Science* **1990**, *249*, 505-510.

(29) Ellington, A. D.; Szostak, J. W. Invitro Selection of Rna Molecules that Bind Specific Ligands. *Nature* **1990**, *346*, 818-822.

(30) Robertson, D. L.; Joyce, G. F. Selection Invitro of an Rna Enzyme that Specifically Cleaves Single-Stranded-Dna. *Nature* **1990**, *344*, 467-468.

(31) Nutiu, R.; Li, Y. F. Structure-switching signaling aptamers: Transducing molecular recognition into fluorescence signaling. *Chemistry-a European Journal* **2004**, *10*, 1868-1876.

(32) Klussmann, S., Ed.; In *The Aptamer Handbook: Functional Oligonucleotides and Their Applications;* Wiley-VCH: **2006**; pp 518.

(33) Jayasena, S. D. Aptamers: An emerging class of molecules that rival antibodies in diagnostics. *Clin. Chem.* **1999**, *45*, 1628-1650.

(34) O'Sullivan, C. K. Aptasensors - the future of biosensing. *Analytical and Bioanalytical Chemistry* **2002**, *372*, 44-48.

(35) Bunka, D. H. J.; Stockley, P. G. Aptamers come of age - at last. *Nature Reviews Microbiology* **2006**, *4*, 588-596.

(36) Haes, A. J.; Van Duyne, R. P. A nanoscale optical blosensor: Sensitivity and selectivity of an approach based on the localized surface plasmon resonance spectroscopy of triangular silver nanoparticles. *J. Am. Chem. Soc.* **2002**, *124*, 10596-10604.

(37) Hrapovic, S.; Liu, Y. L.; Male, K. B.; Luong, J. H. T. Electrochemical biosensing platforms using platinum nanoparticles and carbon nanotubes. *Anal. Chem.* **2004**, *76*, 1083-1088.

(38) Wang, J.; Xu, D. K.; Kawde, A. N.; Polsky, R. Metal nanoparticle-based electrochemical stripping potentiometric detection of DNA hybridization. *Anal. Chem.* **2001**, *73*, 5576-5581.

(39) Katz, E.; Willner, I. Probing biomolecular interactions at conductive and semiconductive surfaces by impedance spectroscopy: Routes to impedimetric immunosensors, DNA-Sensors, and enzyme biosensors. *Electroanalysis* **2003**, *15*, 913-947.

(40) Gerard, M.; Chaubey, A.; Malhotra, B. D. Application of conducting polymers to biosensors. *Biosens. Bioelectron.* **2002**, *17*, 345-359.

(41) Jiang, P. J.; Guo, Z. J. Fluorescent detection of zinc in biological systems: recent development on the design of chemosensors and biosensors. *Coord. Chem. Rev.* **2004**, *248*, 205-229.

(42) Russell, R. J.; Pishko, M. V.; Gefrides, C. C.; McShane, M. J.; Cote, G. L. A fluorescence-based glucose biosensor using concanavalin A and dextran encapsulated in a poly(ethylene glycol) hydrogel. *Anal. Chem.* **1999**, *71*, 3126-3132.

(43) Liu, J. W.; Lu, Y. A colorimetric lead biosensor using DNAzyme-directed assembly of gold nanoparticles. *J. Am. Chem. Soc.* **2003**, *125*, 6642-6643.

(44) Nath, N.; Chilkoti, A. A colorimetric gold nanoparticle sensor to interrogate biomolecular interactions in real time on a surface. *Anal. Chem.* **2002**, *74*, 504-509.

(45) Nutiu, R.; Li, Y. F. Aptamers with fluorescence-signaling properties. *Methods* **2005**, *37*, 16-25.

(46) Nutiu, R.; Li, Y. F. Structure-switching signaling aptamers. *J. Am. Chem. Soc.* **2003**, *125*, 4771-4778.

(47) Nutiu, R.; Mei, S.; Liu, Z. J.; Li, Y. F. Engineering DNA aptamers and DNA enzymes with fluorescence-signaling properties. *Pure and Applied Chemistry* **2004**, *76*, 1547-1561.

(48) Liss, M.; Petersen, B.; Wolf, H.; Prohaska, E. An aptamer-based quartz crystal protein biosensor. *Anal. Chem.* **2002**, *74*, 4488-4495.

(49) Liu, J. W.; Lu, Y. Fast colorimetric sensing of adenosine and cocaine based on a general sensor design involving aptamers and nanoparticles. *Angewandte Chemie-International Edition* **2006**, *45*, 90-94.

(50) Pavlov, V.; Xiao, Y.; Shlyahovsky, B.; Willner, I. Aptamer-functionalized Au nanoparticles for the amplified optical detection of thrombin. *J. Am. Chem. Soc.* **2004**, *126*, 11768-11769.

(51) McCauley, T. G.; Hamaguchi, N.; Stanton, M. Aptamer-based biosensor arrays for detection and quantification of biological macromolecules. *Anal. Biochem.* **2003**, *319*, 244-250.

(52) Pavlov, V.; Shlyahovsky, B.; Willner, I. Fluorescence detection of DNA by the catalytic activation of an aptamer/thrombin complex. *J. Am. Chem. Soc.* **2005**, *127*, 6522-6523.

(53) Potyrailo, R. A.; Conrad, R. C.; Ellington, A. D.; Hieftje, G. M. Adapting selected nucleic acid ligands (aptamers) to biosensors. *Anal. Chem.* **1998**, *70*, 3419-3425.

(54) Herr, J. K.; Smith, J. E.; Medley, C. D.; Shangguan, D. H.; Tan, W. H. Aptamer-conjugated nanoparticles for selective collection and detection of cancer cells. *Anal. Chem.* **2006**, *78*, 2918-2924.

(55) Smith, J. E.; Medley, C. D.; Tang, Z.; Shangguan, D.; Lofton, C.; Tan, W. Aptamer-conjugated nanoparticles for the collection and detection of multiple cancer cells. *Anal. Chem.* **2007**, *79*, 3075-3082.

(56) Ho, H. A.; Leclerc, M. Optical sensors based on hybrid aptamer/conjugated polymer complexes. *J. Am. Chem. Soc.* **2004**, *126*, 1384-1387.

(57) Lim, S. H.; Bestvater, F.; Buchy, P.; Mardy, S.; Yu, A. D. C. Quantitative Analysis of Nucleic Acid Hybridization on Magnetic Particles and Quantum Dot-Based Probes. *Sensors* **2009**, *9*, 5590-5599.

(58) Xu, H. X.; Sha, M. Y.; Wong, E. Y.; Uphoff, J.; Xu, Y. H.; Treadway, J. A.; Truong, A.; O'Brien, E.; Asquith, S.; Stubbins, M.; Spurr, N. K.; Lai, E. H.; Mahoney, W. Multiplexed SNP genotyping using the Qbead (TM) system: a quantum dot-encoded microsphere-based assay. *Nucleic Acids Res.* **2003**, *31*, e43.

(59) Huang, P. J.; Liu, J. Flow Cytometry-Assisted Detection of Adenosine in Serum with an Immobilized Aptamer Sensor. *Anal. Chem.* **2010**, *82*, 4020-4026.

(60) Huang, P. J.; Liu, J. Immobilization of DNA on Magnetic Microparticles for Mercury Enrichment and Detection with Flow Cytometry. *Chemistry-a European Journal* **2011**, *17*, 5003-5009.

(61) Kwon, Y.; Hara, C. A.; Knize, M. G.; Hwang, M. H.; Venkateswaran, K. S.; Wheeler, E. K.; Bell, P. M.; Renzi, R. F.; Fruetel, J. A.; Bailey, C. G. Magnetic Bead Based Immunoassay for Autonomous Detection of Toxins. *Anal. Chem.* **2008**, *80*, 8416-8423.

(62) Tennico, Y. H.; Hutanu, D.; Koesdjojo, M. T.; Bartel, C. M.; Remcho, V. T. On-Chip Aptamer-Based Sandwich Assay for Thrombin Detection Employing Magnetic Beads and Quantum Dots. *Anal. Chem.* **2010**, *82*, 5591-5597.

(63) Centi, S.; Tombelli, S.; Minunni, M.; Mascini, M. Aptamer-based detection of plasma proteins by an electrochemical assay coupled to magnetic beads. *Anal. Chem.* **2007**, *79*, 1466-1473.

(64) Balamurugan, S.; Obubuafo, A.; Soper, S. A.; Spivak, D. A. Surface immobilization methods for aptamer diagnostic applications. *Analytical and Bioanalytical Chemistry* **2008**, *390*, 1009-1021.

(65) Herne, T. M.; Tarlov, M. J. Characterization of DNA probes immobilized on gold surfaces. *J. Am. Chem. Soc.* **1997**, *119*, 8916-8920.

(66) Love, J. C.; Estroff, L. A.; Kriebel, J. K.; Nuzzo, R. G.; Whitesides, G. M. Self-assembled monolayers of thiolates on metals as a form of nanotechnology. *Chem. Rev.* **2005**, *105*, 1103-1169.

(67) Farokhzad, O. C.; Jon, S. Y.; Khademhosseini, A.; Tran, T. N. T.; LaVan, D. A.; Langer, R. Nanopartide-aptamer bioconjugates: A new approach for targeting prostate cancer cells. *Cancer Res.* **2004**, *64*, 7668-7672.

(68) Gronewold, T. M. A.; Glass, S.; Quandt, E.; Famulok, M. Monitoring complex formation in the blood-coagulation cascade using aptamer-coated SAW sensors. *Biosens. Bioelectron.* **2005**, *20*, 2044-2052.

(69) Schlensog, M. D.; Gronewold, T. M. A.; Tewes, M.; Famulok, M.; Quandt, E. A Love-wave biosensor using nucleic acids as ligands. *Sensors and Actuators B-Chemical* **2004**, *101*, 308-315.

(70) Weber, P. C.; Ohlendorf, D. H.; Wendoloski, J. J.; Salemme, F. R. Structural Origins of High-Affinity Biotin Binding to Streptavidin. *Science* **1989**, *243*, 85-88.

(71) Shao, Y.; Wang, J.; Wu, H.; Liu, J.; Aksay, I. A.; Lin, Y. Graphene Based Electrochemical Sensors and Biosensors: A Review. *Electroanalysis* **2010**, *22*, 1027-1036.

(72) Novoselov, K.; Geim, A.; Morozov, S.; Jiang, D.; Zhang, Y.; Dubonos, S.; Grigorieva, I.; Firsov, A. Electric field effect in atomically thin carbon films. *Science* **2004**, *306*, 666-669.

(73) Geim, A. K.; Novoselov, K. S. The rise of graphene. *Nature Materials* **2007**, *6*, 183-191.

(74) Allen, M. J.; Tung, V. C.; Kaner, R. B. Honeycomb Carbon: A Review of Graphene. *Chem. Rev.* **2010**, *110*, 132-145.

(75) Rao, C. N. R.; Sood, A. K.; Subrahmanyam, K. S.; Govindaraj, A. Graphene: The New Two-Dimensional Nanomaterial. *Angewandte Chemie-International Edition* **2009**, *48*, 7752-7777.

(76) Singh, V.; Joung, D.; Zhai, L.; Das, S.; Khondaker, S. I.; Seal, S. Graphene based materials: Past, present and future. *Progress in Materials Science* **2011**, *56*, 1178-1271.

(77) Castro Neto, A. H.; Guinea, F.; Peres, N. M. R.; Novoselov, K. S.; Geim, A. K. The electronic properties of graphene RID B-9537-2008. *Reviews of Modern Physics* **2009**, *81*, 109-162.

(78) Chen, D.; Tang, L.; Li, J. Graphene-based materials in electrochemistry. *Chem. Soc. Rev.* **2010**, *39*, 3157-3180.

(79) Geim, A. K. Graphene: Status and Prospects. *Science* **2009**, *324*, 1530-1534.

(80) Park, S.; Ruoff, R. S. Chemical methods for the production of graphenes. *Nature Nanotechnology* **2009**, *4*, 217-224.

(81) Hummers, W. S.; Offeman, R. E. Preparation of Graphitic Oxide. *J. Am. Chem. Soc.* **1958**, *80*, 1339-1339.

(82) Marcano, D. C.; Kosynkin, D. V.; Berlin, J. M.; Sinitskii, A.; Sun, Z.; Slesarev, A.; Alemany, L. B.; Lu, W.; Tour, J. M. Improved Synthesis of Graphene Oxide. *Acs Nano* **2010**, *4*, 4806-4814.

(83) Berger, C.; Song, Z.; Li, X.; Wu, X.; Brown, N.; Naud, C.; Mayou, D.; Li, T.; Hass, J.; Marchenkov, A. N.; Conrad, E. H.; First, P. N.; de Heer, W. A. Electronic confinement and coherence in patterned epitaxial graphene. *Science* **2006**, *312*, 1191-1196.

(84) Emtsev, K. V.; Bostwick, A.; Horn, K.; Jobst, J.; Kellogg, G. L.; Ley, L.; McChesney, J. L.; Ohta, T.; Reshanov, S. A.; Roehrl, J.; Rotenberg, E.; Schmid, A. K.; Waldmann, D.; Weber, H. B.; Seyller, T. Towards wafer-size graphene layers by atmospheric pressure graphitization of silicon carbide. *Nature Materials* **2009**, *8*, 203-207.

(85) Sutter, P. W.; Flege, J.; Sutter, E. A. Epitaxial graphene on ruthenium. *Nature Materials* **2008**, *7*, 406-411.

(86) Li, X.; Cai, W.; An, J.; Kim, S.; Nah, J.; Yang, D.; Piner, R.; Velamakanni, A.; Jung, I.; Tutuc, E.; Banerjee, S. K.; Colombo, L.; Ruoff, R. S. Large-Area Synthesis of High-Quality and Uniform Graphene Films on Copper Foils. *Science* **2009**, *324*, 1312-1314.

(87) Reina, A.; Jia, X.; Ho, J.; Nezich, D.; Son, H.; Bulovic, V.; Dresselhaus, M. S.; Kong, J. Large Area, Few-Layer Graphene Films on Arbitrary Substrates by Chemical Vapor Deposition. *Nano Letters* **2009**, *9*, 30-35.

(88) Schedin, F.; Geim, A. K.; Morozov, S. V.; Hill, E. W.; Blake, P.; Katsnelson, M. I.; Novoselov, K. S. Detection of individual gas molecules adsorbed on graphene. *Nature Materials* **2007**, *6*, 652-655.

(89) Shan, C.; Yang, H.; Han, D.; Zhang, Q.; Ivaska, A.; Niu, L. Electrochemical determination of NADH and ethanol based on ionic liquid-functionalized graphene. *Biosens. Bioelectron.* **2010**, *25*, 1504-1508.

(90) Zhou, M.; Zhai, Y.; Dong, S. Electrochemical Sensing and Biosensing Platform Based on Chemically Reduced Graphene Oxide. *Anal. Chem.* **2009**, *81*, 5603-5613.

(91) Ohno, Y.; Maehashi, K.; Yamashiro, Y.; Matsumoto, K. Electrolyte-Gated Graphene Field-Effect Transistors for Detecting pH Protein Adsorption. *Nano Letters* **2009**, *9*, 3318-3322.

(92) Wang, Y.; Li, Y.; Tang, L.; Lu, J.; Li, J. Application of graphene-modified electrode for selective detection of dopamine. *Electrochemistry Communications* **2009**, *11*, 889-892.

(93) Lu, J.; Do, I.; Drzal, L. T.; Worden, R. M.; Lee, I. Nanometal-decorated exfoliated graphite nanoplatelet based glucose biosensors with high sensitivity and fast response. *Acs Nano* **2008**, *2*, 1825-1832.

(94) Shan, C.; Yang, H.; Song, J.; Han, D.; Ivaska, A.; Niu, L. Direct Electrochemistry of Glucose Oxidase and Biosensing for Glucose Based on Graphene. *Anal. Chem.* **2009**, *81*, 2378-2382.

(95) Li, J.; Guo, S.; Zhai, Y.; Wang, E. High-sensitivity determination of lead and cadmium based on the Nafion-graphene composite film. *Anal. Chim. Acta* **2009**, *649*, 196-201.

(96) Li, J.; Guo, S.; Zhai, Y.; Wang, E. Nafion-graphene nanocomposite film as enhanced sensing platform for ultrasensitive determination of cadmium. *Electrochemistry Communications* **2009**, *11*, 1085-1088.

(97) Dong, X.; Shi, Y.; Huang, W.; Chen, P.; Li, L. Electrical Detection of DNA Hybridization with Single-Base Specificity Using Transistors Based on CVD-Grown Graphene Sheets. *Adv Mater* **2010**, *22*, 1649-1653.

(98) Mohanty, N.; Berry, V. Graphene-Based Single-Bacterium Resolution Biodevice and DNA Transistor: Interfacing Graphene Derivatives with Nanoscale and Microscale Biocomponents. *Nano Letters* **2008**, *8*, 4469-4476.

(99) Loh, K. P.; Bao, Q.; Eda, G.; Chhowalla, M. Graphene oxide as a chemically tunable platform for optical applications. *Nature Chemistry* **2010**, *2*, 1015-1024.

(100) Kagan, M. R.; Mccreery, R. L. Reduction of Fluorescence Interference in Raman-Spectroscopy Via Analyte Adsorption on Graphitic Carbon. *Anal. Chem.* **1994**, *66*, 4159-4165.

(101) Dong, H.; Gao, W.; Yan, F.; Ji, H.; Ju, H. Fluorescence Resonance Energy Transfer between Quantum Dots and Graphene Oxide for Sensing Biomolecules. *Anal. Chem.* **2010**, *82*, 5511-5517.

(102) Xie, L.; Ling, X.; Fang, Y.; Zhang, J.; Liu, Z. Graphene as a Substrate To Suppress Fluorescence in Resonance Raman Spectroscopy. *J. Am. Chem. Soc.* **2009**, *131*, 9890-9891.

(103) He, S.; Song, B.; Li, D.; Zhu, C.; Qi, W.; Wen, Y.; Wang, L.; Song, S.; Fang, H.; Fan, C. A Graphene Nanoprobe for Rapid, Sensitive, and Multicolor Fluorescent DNA Analysis. *Adv. Funct. Mater.* **2010**, *20*, 453-459.

(104) Lu, C.; Yang, H.; Zhu, C.; Chen, X.; Chen, G. A Graphene Platform for Sensing Biomolecules. *Angew. Chem. Int. Ed.* **2009**, *48*, 4785-4787.

(105) Jang, H.; Kim, Y.; Kwon, H.; Yeo, W.; Kim, D.; Min, D. A Graphene-Based Platform for the Assay of Duplex-DNA Unwinding by Helicase. *Angew. Chem. Int. Ed.* **2010**, *49*, 5703-5707.

(106) Li, F.; Huang, Y.; Yang, Q.; Zhong, Z.; Li, D.; Wang, L.; Song, S.; Fan, C. A graphene-enhanced molecular beacon for homogeneous DNA detection. *Nanoscale* **2010**, *2*, 1021-1026.

(107) Liu, F.; Choi, J. Y.; Seo, T. S. Graphene oxide arrays for detecting specific DNA hybridization by fluorescence resonance energy transfer. *Biosensors and Bioelectronics* **2010**, *25*, 2361-2365.

(108) Lu, C.; Li, J.; Liu, J.; Yang, H.; Chen, X.; Chen, G. Increasing the Sensitivity and Single-Base Mismatch Selectivity of the Molecular Beacon Using Graphene Oxide as the "Nanoquencher". *Chem. Eur. J.* **2010**, *16*, 4889-4894.

(109) Wu, W.; Hu, H.; Li, F.; Wang, L.; Gao, J.; Lu, J.; Fan, C. A graphene oxide-based nano-beacon for DNA phosphorylation analysis. *Chemical Communications* **2011**, *47*, 1201-1203.

(110) Chang, H.; Tang, L.; Wang, Y.; Jiang, J.; Li, J. Graphene Fluorescence Resonance Energy Transfer Aptasensor for the Thrombin Detection. *Anal. Chem.* **2010**, *82*, 2341-2346.

(111) Wang, X.; Wang, C.; Qu, K.; Song, Y.; Ren, J.; Miyoshi, D.; Sugimoto, N.; Qu, X. Ultrasensitive and Selective Detection of a Prognostic Indicator in Early-Stage Cancer

Using Graphene Oxide and Carbon Nanotubes. *Advanced Functional Materials* **2010**, *20*, 3967-3971.

(112) Jung, J.; Cheon, D.; Liu, F.; Lee, K.; Seo, T. A Graphene Oxide Based Immuno-biosensor for Pathogen Detection. *Angew. Chem. Int. Ed.* **2010**, *49*, 5708-5711.

(113) Wen, Y.; Xing, F.; He, S.; Song, S.; Wang, L.; Long, Y.; Li, D.; Fan, C. A graphene-based fluorescent nanoprobe for silver(i) ions detection by using graphene oxide and a silver-specific oligonucleotide. *Chem. Commun.* **2010**, *46*, 2596-2598.

(114) Zhang, M.; Yin, B.; Tan, W.; Ye, B. A versatile graphene-based fluorescence "on/off" switch for multiplex detection of various targets. *Biosensors and Bioelectronics* **2011**, *26*, 3260-3265.

(115) Song, Y.; Qu, K.; Zhao, C.; Ren, J.; Qu, X. Graphene Oxide: Intrinsic Peroxidase Catalytic Activity and Its Application to Glucose Detection. *Adv Mater* **2010**, *22*, 2206-2210.

(116) Wang, Y.; Li, Z.; Hu, D.; Lin, C.; Li, J.; Lin, Y. Aptamer/Graphene Oxide Nanocomplex for in Situ Molecular Probing in Living Cells. *J. Am. Chem. Soc.* **2010**, *132*, 9274-9276.

(117) Lu, C.; Li, J.; Lin, M.; Wang, Y.; Yang, H.; Chen, X.; Chen, G. Amplified Aptamer-Based Assay through Catalytic Recycling of the Analyte. *Angewandte Chemie-International Edition* **2010**, *49*, 8454-8457.

(118) Sheng, L.; Ren, J.; Miao, Y.; Wang, J.; Wang, E. PVP-coated graphene oxide for selective determination of ochratoxin A via quenching fluorescence of free aptamer. *Biosensors and Bioelectronics* **2011**, *26*, 3494-3499.

(119) Liu, C.; Wang, Z.; Jia, H.; Li, Z. Efficient fluorescence resonance energy transfer between upconversion nanophosphors and graphene oxide: a highly sensitive biosensing platform. *Chem. Commun.* **2011**, *47*, 4661-4663.

(120) Liu, Z.; Robinson, J. T.; Sun, X.; Dai, H. PEGylated Nanographene Oxide for Delivery of Water-Insoluble Cancer Drugs. *J. Am. Chem. Soc.* **2008**, *130*, 10876-10877.

(121) Sun, X.; Liu, Z.; Welsher, K.; Robinson, J. T.; Goodwin, A.; Zaric, S.; Dai, H. Nano-Graphene Oxide for Cellular Imaging and Drug Delivery. *Nano Research* **2008**, *1*, 203-212.

(122) Lu, C.; Zhu, C.; Li, J.; Liu, J.; Chen, X.; Yang, H. Using graphene to protect DNA from cleavage during cellular delivery. *Chem. Commun.* **2010**, *46*, 3116-3118.

(123) Tang, Z.; Wu, H.; Cort, J. R.; Buchko, G. W.; Zhang, Y.; Shao, Y.; Aksay, I. A.; Liu, J.; Lin, Y. Constraint of DNA on Functionalized Graphene Improves its Biostability and Specificity. *Small* **2010**, *6*, 1205-1209.

(124) Feng, L.; Zhang, S.; Liu, Z. Graphene based gene transfection. *Nanoscale* **2011**, *3*, 1252-1257.

(125) Yang, K.; Zhang, S.; Zhang, G.; Sun, X.; Lee, S.; Liu, Z. Graphene in Mice: Ultrahigh In Vivo Tumor Uptake and Efficient Photothermal Therapy. *Nano Lett.* **2010**, *10*, 3318-3323.

(126) Yang, X.; Zhang, X.; Ma, Y.; Huang, Y.; Wang, Y.; Chen, Y. Superparamagnetic graphene oxide-Fe(3)O(4) nanoparticles hybrid for controlled targeted drug carriers. *Journal of Materials Chemistry* **2009**, *19*, 2710-2714.

(127) Yang, X.; Zhang, X.; Liu, Z.; Ma, Y.; Huang, Y.; Chen, Y. High-Efficiency Loading and Controlled Release of Doxorubicin Hydrochloride on Graphene Oxide. *Journal of Physical Chemistry C* **2008**, *112*, 17554-17558.

(128) Wang, Y.; Li, Z.; Wang, J.; Li, J.; Lin, Y. Graphene and graphene oxide: biofunctionalization and applications in biotechnology. *Trends Biotechnol.* **2011**, *29*, 205-212.

(129) Dong, L.; Joseph, K. L.; Witkowski, C. M.; Craig, M. M. Cytotoxicity of single-walled carbon nanotubes suspended in various surfactants. *Nanotechnology* **2008**, *19*, 255702.

(130) Manohar, S.; Mantz, A. R.; Bancroft, K. E.; Hui, C.; Jagota, A.; Vezenov, D. V. Peeling Single-Stranded DNA from Graphite Surface to Determine Oligonucleotide Binding Energy by Force Spectroscopy. *Nano Letters* **2008**, *8*, 4365-4372.

(131) Varghese, N.; Mogera, U.; Govindaraj, A.; Das, A.; Maiti, P. K.; Sood, A. K.; Rao, C. N. R. Binding of DNA Nucleobases and Nucleosides with Graphene RID B-1569-2009. *Chemphyschem* **2009**, *10*, 206-210.

(132) Ortmann, F.; Schmidt, W.; Bechstedt, F. Attracted by long-range electron correlation: Adenine on graphite. *Phys. Rev. Lett.* **2005**, *95*, 186101.

(133) Gowtham, S.; Scheicher, R. H.; Ahuja, R.; Pandey, R.; Karna, S. P. Physisorption of nucleobases on graphene: Density-functional calculations RID A-8759-2009. *Physical Review B* **2007**, *76*, 033401.

(134) Antony, J.; Grimme, S. Structures and interaction energies of stacked graphene-nucleobase complexes RID B-2873-2010. *Physical Chemistry Chemical Physics* **2008**, *10*, 2722-2729.

(135) Zheng, M.; Jagota, A.; Semke, E.; Diner, B.; Mclean, R.; Lustig, S.; Richardson, R.; Tassi, N. DNA-assisted dispersion and separation of carbon nanotubes. *Nature Materials* **2003**, *2*, 338-342.

(136) Zhao, X.; Johnson, J. K. Simulation of adsorption of DNA on carbon nanotubes. *J. Am. Chem. Soc.* **2007**, *129*, 10438-10445.

(137) Jeng, E. S.; Barone, P. W.; Nelson, J. D.; Strano, M. S. Hybridization kinetics and thermodynamics of DNA adsorbed to individually dispersed single-walled carbon nanotubes. *Small* **2007**, *3*, 1602-1609.

(138) Zhen, S. J.; Chen, L. Q.; Xiao, S. J.; Li, Y. F.; Hu, P. P.; Zhan, L.; Peng, L.; Song, E. Q.; Huang, C. Z. Carbon Nanotubes as a Low Background Signal Platform for a Molecular Aptamer Beacon on the Basis of Long-Range Resonance Energy Transfer. *Anal. Chem.* **2010**, *82*, 8432-8437.

(139) Lucrecia Carot, M.; Torresi, R. M.; Garcia, C. D.; Jose Esplandiu, M.; Giacomelli, C. E. Electrostatic and Hydrophobic Interactions Involved in CNT Biofunctionalization with Short ss-DNA. *Journal of Physical Chemistry C* **2010**, *114*, 4459-4465.

(140) Husale, S.; Sahoo, S.; Radenovic, A.; Traversi, F.; Annibale, P.; Kis, A. ssDNA Binding Reveals the Atomic Structure of Graphene. *Langmuir* **2010**, *26*, 18078-18082.

(141) Wu, M.; Kempaiah, R.; Huang, P. J.; Maheshwari, V.; Liu, J. Adsorption and Desorption of DNA on Graphene Oxide Studied by Fluorescently Labeled Oligonucleotides. *Langmuir* **2011**, *27*, 2731-2738.

(142) Mkhoyan, K. A.; Contryman, A. W.; Silcox, J.; Stewart, D. A.; Eda, G.; Mattevi, C.; Miller, S.; Chhowalla, M. Atomic and Electronic Structure of Graphene-Oxide. *Nano Letters* **2009**, *9*, 1058-1063.

(143) Ladbury, J. E.; Chowdhry, B. Z. Sensing the heat: The application of isothermal titration calorimetry to thermodynamic studies of biomolecular interactions. *Chem. Biol.* **1996**, *3*, 791-801.

(144) Gomez-Navarro, C.; Meyer, J. C.; Sundaram, R. S.; Chuvilin, A.; Kurasch, S.; Burghard, M.; Kern, K.; Kaiser, U. Atomic Structure of Reduced Graphene Oxide. *Nano Letters* **2010**, *10*, 1144-1148.

(145) Tinland, B.; Pluen, A.; Sturm, J.; Weill, G. Persistence length of single-stranded DNA. *Macromolecules* **1997**, *30*, 5763-5765.

(146) Li, H.; Rothberg, L. Colorimetric detection of DNA sequences based on electrostatic interactions with unmodified gold nanoparticles. *Proc. Natl. Acad. Sci. U. S. A.* **2004**, *101*, 14036-14039.

(147) Li, H.; Rothberg, L. DNA sequence detection using selective fluorescence quenching of tagged oligonucleotide probes by gold nanoparticles. *Anal. Chem.* **2004**, *76*, 5414-5417.

(148) Li, H.; Rothberg, L. Label-free colorimetric detection of specific sequences in genomic DNA amplified by the polymerase chain reaction. *J. Am. Chem. Soc.* **2004**, *126*, 10958-10961.

(149) Liu, S.; Ghosh, K.; Muthukumar, M. Polyelectrolyte solutions with added salt: A simulation study. *J. Chem. Phys.* **2003**, *119*, 1813-1823.

(150) Rowatt, E.; Williams, R. The Binding of Polyamines and Magnesium to Dna. *J. Inorg. Biochem.* **1992**, *46*, 87-97.

(151) Ren, H.; Wang, C.; Zhang, J.; Zhou, X.; Xu, D.; Zheng, J.; Guo, S.; Zhang, J. DNA Cleavage System of Nanosized Graphene Oxide Sheets and Copper Ions. *ACS Nano* **2010**, *4*, 7169-7174.

(152) Langley, L.; Villanueva, D.; Fairbrother, D. Quantification of surface oxides on carbonaceous materials. *Chemistry of Materials* **2006**, *18*, 169-178.

(153) Damodaran, S. Adsorbed layers formed from mixtures of proteins. *Current Opinion in Colloid & Interface Science* **2004**, *9*, 328-339.

(154) Li, G.; Jiang, Y.; Huang, K.; Ding, P.; Yao, L. Kinetics of adsorption of Saccharomyces cerevisiae mandelated dehydrogenase on magnetic Fe3O4-chitosan nanoparticles. *Colloids and Surfaces A-Physicochemical and Engineering Aspects* **2008**, *320*, 11-18.

(155) Wu, C.; Zhou, Y.; Miao, X.; Ling, L. A novel fluorescent biosensor for sequence-specific recognition of double-stranded DNA with the platform of graphene oxide. *Analyst* **2011**, *136*, 2106-2110.

(156) Huizenga, D.; Szostak, J. A Dna Aptamer that Binds Adenosine and Atp. *Biochemistry (N. Y.)* **1995**, *34*, 656-665.

(157) Neves, M. A. D.; Reinstein, O.; Saad, M.; Johnson, P. E. Defining the secondary structural requirements of a cocaine-binding aptamer by a thermodynamic and mutation study. *Biophys. Chem.* **2010**, *153*, 9-16.

(158) Neves, M. A. D.; Reinstein, O.; Johnson, P. E. Defining a Stem Length-Dependent Binding Mechanism for the Cocaine-Binding Aptamer. A Combined NMR and Calorimetry Study. *Biochemistry (N. Y.)* **2010**, *49*, 8478-8487.

(159) Ono, A.; Togashi, H. Highly selective oligonucleotide-based sensor for mercury(II) in aqueous solutions. *Angewandte Chemie-International Edition* **2004**, *43*, 4300-4302.

(160) Miyake, Y.; Togashi, H.; Tashiro, M.; Yamaguchi, H.; Oda, S.; Kudo, M.; Tanaka, Y.; Kondo, Y.; Sawa, R.; Fujimoto, T.; Machinami, T.; Ono, A. Mercury(II)-mediated formation of thymine-Hg-II-thymine base pairs in DNA duplexes. *J. Am. Chem. Soc.* **2006**, *128*, 2172-2173.

(161) Lytton-Jean, A.; Mirkin, C. A thermodynamic investigation into the binding properties of DNA functionalized gold nanoparticle probes and molecular fluorophore probes. *J. Am. Chem. Soc.* **2005**, *127*, 12754-12755.

(162) Swathi, R. S.; Sebastian, K. L. Excitation energy transfer from a fluorophore to single-walled carbon nanotubes. *J. Chem. Phys.* **2010**, *132*, 104502.

(163) Heller, D.; Jeng, E.; Yeung, T.; Martinez, B.; Moll, A.; Gastala, J.; Strano, M. Optical detection of DNA conformational polymorphism on single-walled carbon nanotubes RID A-4283-2008. *Science* **2006**, *311*, 508-511.

(164) Swathi, R. S.; Sebastian, K. L. Resonance energy transfer from a dye molecule to graphene. *J. Chem. Phys.* **2008**, *129*, 054703.

(165) Swathi, R. S.; Sebastian, K. L. Long range resonance energy transfer from a dye molecule to graphene has (distance)(-4) dependence. *J. Chem. Phys.* **2009**, *130*, 086101.

(166) Swathi, R. S.; Sebastian, K. L. Distance dependence of fluorescence resonance energy transfer. *Journal of Chemical Sciences* **2009**, *121*, 777-787.

(167) Yun, C.; Javier, A.; Jennings, T.; Fisher, M.; Hira, S.; Peterson, S.; Hopkins, B.; Reich, N.; Strouse, G. Nanometal surface energy transfer in optical rulers, breaking the FRET barrier. *J. Am. Chem. Soc.* **2005**, *127*, 3115-3119.

(168) Jennings, T.; Singh, M.; Strouse, G. Fluorescent lifetime quenching near d=1.5 nm gold nanoparticles: Probing NSET validity. *J. Am. Chem. Soc.* **2006**, *128*, 5462-5467.

(169) Sen, T.; Patra, A. Resonance energy transfer from rhodamine 6G to gold nanoparticles by steady-state and time-resolved spectroscopy. *Journal of Physical Chemistry C* **2008**, *112*, 3216-3222.

(170) Chen, Y.; O'Donoghue, M. B.; Huang, Y.; Kang, H.; Phillips, J. A.; Chen, X.; Estevez, M. -.; Yang, C. J.; Tan, W. A Surface Energy Transfer Nanoruler for Measuring Binding Site Distances on Live Cell Surfaces. *J. Am. Chem. Soc.* **2010**, *132*, 16559-16570.

(171) Hagerman, P. Flexibility of Dna. *Annu. Rev. Biophys. Biophys. Chem.* **1988**, *17*, 265-286.

(172) Chang, I. P.; Chiang, C.; Hwang, K. C. Preparation of Fluorescent Magnetic Nanodiamonds and Cellular Imaging. *J. Am. Chem. Soc.* **2008**, *130*, 15476-15481.

(173) Clegg, R. Fluorescence Resonance Energy-Transfer and Nucleic-Acids. *Meth. Enzymol.* **1992**, *211*, 353-388.

(174) Szabo, T.; Berkesi, O.; Forgo, P.; Josepovits, K.; Sanakis, Y.; Petridis, D.; Dekany, I. Evolution of surface functional groups in a series of progressively oxidized graphite oxides. *Chemistry of Materials* **2006**, *18*, 2740-2749.

(175) Cai, W.; Piner, R. D.; Stadermann, F. J.; Park, S.; Shaibat, M. A.; Ishii, Y.; Yang, D.; Velamakanni, A.; An, S. J.; Stoller, M.; An, J.; Chen, D.; Ruoff, R. S. Synthesis and solid-state NMR structural characterization of C-13-labeled graphite oxide RID A-2790-2009 RID A-2869-2009 RID B-7605-2009. *Science* **2008**, *321*, 1815-1817.

(176) Lerf, A.; He, H.; Forster, M.; Klinowski, J. Structure of graphite oxide revisited. *J Phys Chem B* **1998**, *102*, 4477-4482.

(177) Kudin, K. N.; Ozbas, B.; Schniepp, H. C.; Prud'homme, R. K.; Aksay, I. A.; Car, R. Raman spectra of graphite oxide and functionalized graphene sheets RID A-7723-2008 RID B-8368-2008 RID B-9281-2008. *Nano Letters* **2008**, *8*, 36-41.

(178) Qu, L.; Martin, R.; Huang, W.; Fu, K.; Zweifel, D.; Lin, Y.; Sun, Y.; Bunker, C.; Harruff, B.; Gord, J.; Allard, L. Interactions of functionalized carbon nanotubes with tethered pyrenes in solution. *J. Chem. Phys.* **2002**, *117*, 8089-8094.

(179) Li, H.; Kose, M. E.; Qu, L.; Lin, Y.; Martin, R. B.; Zhou, B.; Harruff, B. A.; Allard, L. F.; Sun, Y. Excited-state energy transfers in single-walled carbon nanotubes functionalized with tethered pyrenes. *Journal of Photochemistry and Photobiology A-Chemistry* **2007**, *185*, 94-100.

(180) Martin, R.; Qu, L.; Lin, Y.; Harruff, B.; Bunker, C.; Gord, J.; Allard, L.; Sun, Y. Functionalized carbon nanotubes with tethered pyrenes: Synthesis and photophysical properties. *J Phys Chem B* **2004**, *108*, 11447-11453.

(181) Lin, C.; Liu, Y.; Yan, H. Designer DNA Nanoarchitectures. *Biochemistry (N. Y.)* **2009**, *48*, 1663-1674.

(182) Pei, H.; Lu, N.; Wen, Y.; Song, S.; Liu, Y.; Yan, H.; Fan, C. A DNA Nanostructure-based Biomolecular Probe Carrier Platform for Electrochemical Biosensing. *Adv Mater* **2010**, *22*, 4754-4758.